Potential of thermal neutrons to correct cosmic-ray neutron soil moisture content measurements for dynamic biomass effects

Jannis Christoph Jakobi[1,1], Johan A. Huisman[2,2], Hannah Fuchs[3,3], Harry Vereecken[1,1], and Heye Bogena[4,4]

[1]Forschungszentrum Jülich GmbH
[2]Forschungszentrum Jülich
[3]Wasserverband Eifel-Rur (WVER)
[4]Forschungszentrum Juelich, GmbH

November 30, 2022

Abstract

Cosmic ray neutron sensors (CRNS) allow to determine field-scale soil moisture content non-invasively due to the dependence of aboveground measured epithermal neutrons on the amount of hydrogen. Because other pools besides soil contain hydrogen (e.g. biomass), it is necessary to consider these for accurate soil moisture content measurements, especially when they are changing dynamically (e.g., arable crops, de- and reforestation). In this study, we compare four approaches for the correction of biomass effects on soil moisture content measurements with CRNS using experiments with three crops (sugar beet, winter wheat and maize) on similar soils: I) site-specific functions based on in-situ measured biomass, II) a generic approach, III) the thermal-to-epithermal neutron ratio (Nr) and IV) the thermal neutron intensity. Calibration of the CRNS during bare soil conditions resulted in root mean square errors (RMSE) of 0.097, 0.041 and 0.019 m3/m3 between estimated and reference soil moisture content of the cropped soils, respectively. Considering in-situ measured biomass for correction reduced the RMSE to 0.015, 0.018 and 0.009 m3/m3. When thermal neutron intensity was considered for correction, similarly accurate results were obtained. Corrections based on Nr and the generic approach were less accurate. We also explored the use of CRNS for biomass estimation. The use of Nr only provided accurate biomass estimates for sugar beet. However, significant site-specific relationships between biomass and thermal neutron intensity were obtained for all three crops. It was concluded that thermal neutron intensity can be used to correct soil moisture content estimates from CRNS and to estimate biomass.

Potential of thermal neutrons to correct cosmic-ray neutron soil moisture content measurements for dynamic biomass effects

J. Jakobi[1],

J. A. Huisman[1],

H. Fuchs[2],

H. Vereecken[1]

H. R. Bogena[1]

[1]Agrosphere Institute (IBG-3), Forschungszentrum Jülich GmbH, Jülich, Germany

[2]Wasserverband Eifel-Rur (WVER), Düren, Germany

Key Points

- Cosmic ray soil moisture content measurements were most accurate when corrected with in-situ biomass or thermal neutron intensity
- The effect of biomass on epithermal and thermal neutron intensity is plant-specific
- Biomass could be estimated from thermal neutron intensity for three crop types, but not with the thermal-to-epithermal neutron ratio

Plain language summary

Water availability is a key challenge in agriculture, especially given the expected increase of droughts related to climate change. A promising non-invasive technique to monitor soil moisture content is cosmic-ray neutron sensing (CRNS), which is based on the negative correlation between the number of near-surface fast neutrons originating from cosmic radiation and the amount of hydrogen stored as soil moisture. However, hydrogen is also stored in other pools, such as biomass. These additional pools of hydrogen must be considered to accurately determine soil moisture content with CRNS. In this study, we used data from three experiments with different crops for comparing four methods for the correction of biomass effects on the measurement of soil moisture content with CRNS. We found that soil moisture content measurements were most accurate when locally measured biomass was considered for correction. We also found that changes in the amount of biomass of different crops can be quantified using thermal neutrons additionally detected by CRNS, i.e. neutrons from cosmic rays that have a lower energy than fast neutrons. A correction of biomass effects using thermal neutron measurements also provided accurate soil moisture content measurements.

Abstract

Cosmic ray neutron sensors (CRNS) allow to determine field-scale soil moisture content non-invasively due to the dependence of aboveground measured epithermal neutrons on the amount of hydrogen. Because other pools besides soil contain hydrogen (e.g. biomass), it is necessary to consider these for accurate soil moisture content measurements, especially when they are changing dynamically (e.g., arable crops, de- and reforestation). In this study, we compare four approaches for the correction of biomass effects on soil moisture content measurements with CRNS using experiments with three crops (sugar beet, winter wheat and maize) on similar soils: I) site-specific functions based on in-situ measured biomass, II) a generic approach, III) the thermal-to-epithermal neutron ratio (N_r) and IV) the thermal neutron intensity. Calibration of the CRNS during bare soil conditions resulted in root mean square errors (RMSE) of 0.097, 0.041 and 0.019 m^3/m^3 between estimated and reference soil moisture content of the cropped soils, respectively. Considering in-situ measured biomass for correction reduced the RMSE to 0.015, 0.018 and 0.009 m^3/m^3. When thermal neutron intensity was considered for correction, similarly accurate results were obtained. Corrections based on N_r and the generic approach were less accurate. We also explored the use of CRNS for biomass estimation. The use of N_r only provided accurate biomass estimates for sugar beet. However, significant site-specific relationships between biomass and thermal neutron intensity were obtained for all three crops. It was concluded that thermal neutron intensity can be used to correct soil moisture content estimates from CRNS and to estimate biomass.

1. Introduction

Cosmic ray neutron (CRN) sensing is a non-invasive method for soil moisture content measurement (ZREDA ET AL., 2008). By now, it has become a widely used method for soil moisture content determination and cosmic ray neutron sensors (CRNS) are operated in more than 200 locations worldwide (BOGENA ET AL., 2015; ANDREASEN ET AL., 2017b), also in regional (e.g., BAATZ ET AL., 2014; BOGENA ET AL., 2018), national (e.g., ZREDA ET AL., 2012; COOPER ET AL., 2021) and continent-wide networks (e.g., BOGENA ET AL., in revision; HAWDON ET AL., 2014). The aboveground epithermal neutron intensity (energy range from ~0.5 eV to 100 keV; ZREDA ET AL., 2008) is inversely related to the hydrogen content of the environment. Since hydrogen is mostly located in soil water in terrestrial environments, the measurement of the aboveground epithermal neutron intensity can be used to estimate soil moisture content (DESILETS ET AL., 2010).The sensing volume of CRNS is much larger compared to most other ground-based soil moisture sensing techniques and corresponds to a cylinder with 130 - 240 m radius and 15 – 83 cm soil depth depending on the soil moisture content (KÖHLI ET AL., 2015; SCHRÖN ET AL., 2017).

It is important to note that hydrogen is also stored in other environmental pools besides soil, which may cause deviations between soil moisture content determined with CRNS and reference measurements. Common additional hydrogen sources are snow (TIAN ET AL., 2016; BOGENA ET AL., 2020), biomass (FRANZ ET AL., 2013b; BAATZ ET AL., 2015; BARONI AND OSWALD, 2015; TIAN ET AL., 2016; FERSCH ET AL., 2018; JAKOBI ET AL., 2018), ponding water (SCHRÖN ET AL., 2017), and interception by vegetation (BARONI AND OSWALD, 2015; ANDREASEN ET AL., 2016; JAKOBI ET AL., 2018) as well as the litter layer (BOGENA ET AL., 2013). The timing of the observed deviations may help to identify the most probable source of additional hydrogen affecting the epithermal neutron intensity. In the absence of snow, earlier CRN sensing studies on agricultural sites typically identified biomass as the most important reason for deviations between the CRNS derived soil moisture content and in-situ measured reference soil moisture content (e.g., BARONI AND OSWALD, 2015; TIAN ET AL., 2016; JAKOBI ET AL., 2018). Thus, the removal of the effect of biomass is crucial for accurate soil moisture content estimation especially on agricultural sites. Although methods to correct soil moisture content for the presence of biomass have

87　been developed (e.g., HAWDON ET AL., 2014; BAATZ ET AL., 2015; JAKOBI ET AL., 2018),
88　they typically require laborious biomass measurements that are often not available.

89　To circumvent the need for laborious biomass measurements for correction, several
90　studies attempted to directly determine the amount of aboveground biomass from
91　epithermal CRNS measurements and in-situ soil moisture content measurements (FRANZ
92　ET AL., 2013b; BARONI AND OSWALD, 2015). More recently, it was shown that the ratio of
93　thermal (≤ 0.5 eV) to epithermal neutron intensity (N_r) can be used to determine
94　aboveground biomass and to correct biomass effects on CRN measurements (TIAN ET
95　AL., 2016; JAKOBI ET AL., 2018). The dependency of N_r on biomass was also confirmed by
96　neutron transport modeling of a forest site (ANDREASEN ET AL., 2017a) and by a
97　comparison of the measured N_r with vegetation indices derived from remote sensing
98　(VATHER ET AL., 2020). However, it has not yet been investigated in detail why N_r depends
99　on biomass and whether N_r-based correction methods can be applied for different
100　vegetation types. Such investigations are particularly important given that the intensity of
101　thermal neutrons also depends on soil moisture content and soil chemistry, since thermal
102　neutrons are particularly strongly absorbed by certain elements in the soil (ZREDA ET AL.,
103　2008; ANDREASEN ET AL., 2016). In addition, recent studies have shown that the sensing
104　volume of thermal neutrons is much smaller than in the case of epithermal neutrons
105　(BOGENA ET AL., 2020; RASCHE ET AL., 2021). Using neutron transport simulations, it was
106　found that thermal neutrons have a radial footprint of approximately 45 m that increases
107　slightly with increasing soil moisture content and a sensing depth that increases from 10
108　to 65 cm with decreasing soil moisture content from $0.50 - 0.01$ m^3/m^3 (JAKOBI ET AL.,
109　2021).

110　The aim of this study is to compare four approaches for the correction of crop biomass
111　effects on CRNS soil moisture content measurements using measurements of thermal
112　and epithermal neutron intensity, reference soil moisture content, as well as biomass
113　development for three crops (sugar beet, maize, and winter wheat). In particular, we
114　considered the following approaches for correction: I) local linear regression models
115　based on epithermal neutron intensity, in-situ soil moisture content and in-situ biomass
116　measurements, II) the empirical generic approach developed by BAATZ ET AL. (2015), III)

117 local linear regression models based on both epithermal neutron and N_r measurements,
118 and IV) local linear regression models based on both epithermal neutron and thermal
119 neutron measurements. In addition, we evaluated to what extent aboveground biomass
120 can be determined from the N_r and from the thermal neutron intensity for the three crops
121 considered in this study.

2. Materials and Methods

2.1. The Selhausen experimental site

124 The Selhausen experimental site is located in western Germany, approximately 40 km
125 west of Cologne (50.865°N, 6.447°E) and is part of the TERENO (TERrestrial
126 ENvironmental Observatories) Rur hydrological observatory (BOGENA ET AL., 2018). The
127 site is located in the temperate maritime climate zone with a mean annual temperature
128 and precipitation of 10.2 °C and 714 mm, respectively (KORRES ET AL., 2015). The
129 experimental site consists of 52 fields managed by local farmers. The main soil type is
130 Cambisol with a silty loam soil texture (RUDOLPH ET AL., 2015; BROGI ET AL., 2019) on top
131 of Pleistocene sand and gravel sediments interrupted by subsurface channels of the
132 Rhine/Meuse river system filled with finer sediment (WEIHERMÜLLER ET AL., 2007). This
133 subsoil heterogeneity leads to characteristic biomass patterns, especially on the sand and
134 gravel dominated fields (compare Figure 1; RUDOLPH ET AL., 2015; BROGI ET AL., 2020).
135 The experiments presented in this study were conducted on three different fields (Figure
136 1) with three different crops and in three years: winter wheat on field F11 in 2015 (FUCHS,
137 2016), sugar beet on field F01 in 2016 (JAKOBI ET AL., 2018) and maize on field F52 in
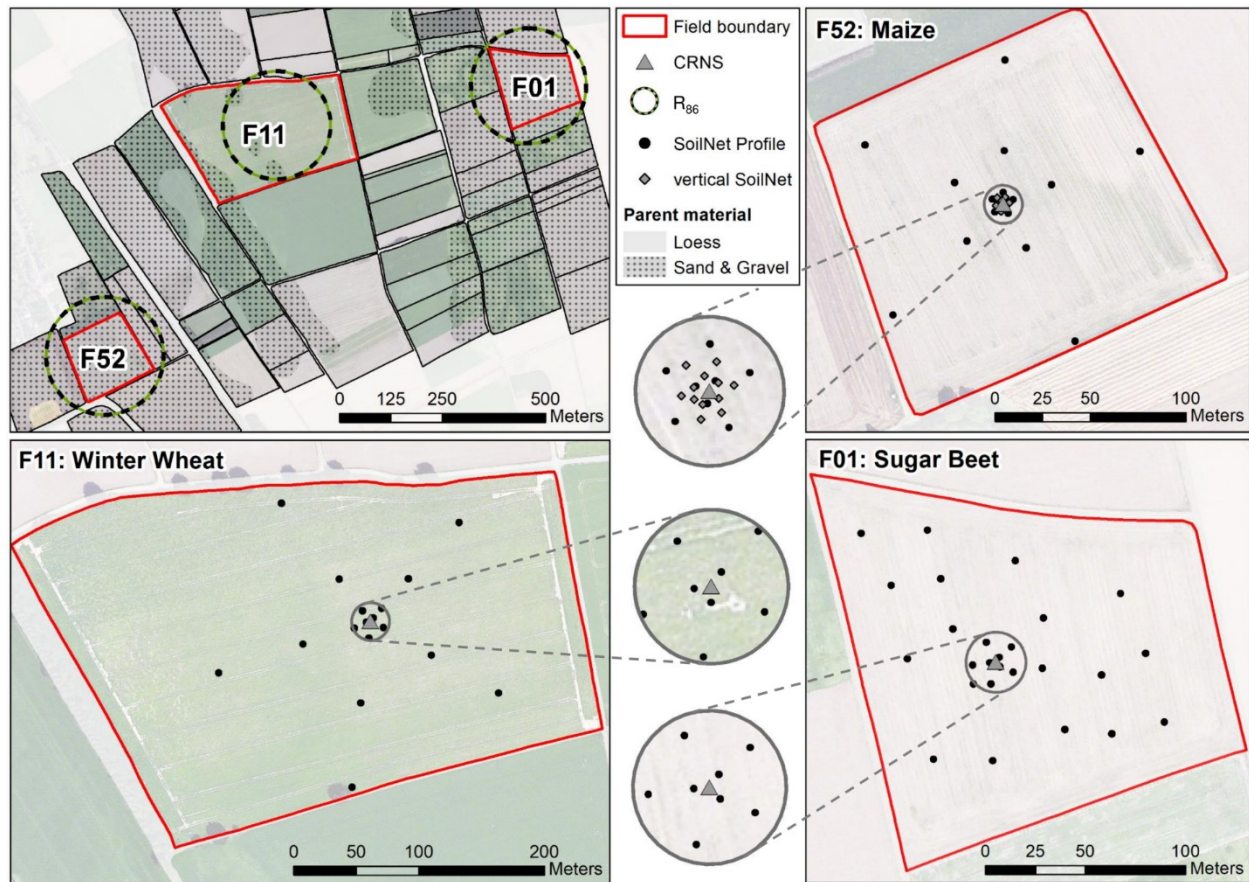138 2018.

Figure 1: Map of the Selhausen experimental site showing an overview of the fields with dominant parent material and the footprint radii (R_{86}) of the three experiments estimated using the average soil moisture content, air humidity, pressure and vegetation height conditions, respectively (i.e., winter wheat: 132 m; sugar beet: 157 m; maize: 146 m). Furthermore, the SoilNet locations within the three fields and magnifications with 15 m radius around the CRNS are shown for winter wheat and sugar beet. For the maize experiment, the magnification shows an area with a 10 m radius around the CRNS. Base maps: ESRI World Imagery and Contributors.

2.2. Auxiliary meteorological data

Air temperature, relative humidity, and atmospheric pressure were measured on-site during the experiments. The absolute humidity necessary for neutron count correction was calculated from relative humidity and air pressure. Data gaps in absolute humidity and atmospheric pressure were filled based on linear regression models obtained for the entire measurement period. For this, time series of the same variables were obtained from a climate station situated next to the CRNS on field site F11 (SE_EC_001, http://teodoor.icg.kfa-juelich.de/ibg3searchportal2/index.jsp, compare Figure 1). Hourly

155 precipitation sums were obtained from a nearby climate station ~400 m northeast of the

156 field site F11 (SE_BDK_002).

2.3. In-situ soil moisture content measurements

158 We used SoilNet wireless sensor networks (BOGENA ET AL., 2010) for obtaining reference

159 in-situ soil moisture content at 18 – 26 locations within each field (Figure 1). At each

160 location, soil moisture content was measured in three depths using two soil moisture

161 content sensors (sugar beet and maize: SMT100, Truebner GmbH, Neustadt, Germany;

162 winter wheat: SPADE, sceme.de GmbH, Horn-Bad Meinberg, Germany). Two sensors

163 were installed at each depth to increase the measurement volume and to identify

164 malfunctioning sensors. Each sensor was calibrated individually to translate the sensor

165 response into dielectric permittivity (BOGENA ET AL., 2017). The measured permittivity was

166 related to soil moisture content with the TOPP ET AL. (1980) equation.

167 The measurement designs at the three field sites differed because of the differently sized

168 fields and to account for the high soil heterogeneity in the case of sugar beet (JAKOBI ET

169 AL., 2018). For winter wheat, we installed sensors at five locations at distances of 11, 50,

170 and 110 m from the CRNS (i.e. 15 locations), as suggested by SCHRÖN ET AL. (2017).

171 Additionally, sensors were installed at three locations at 3 m distance from the CRNS to

172 account for the higher sensitivity near the detector. At all locations, the measurement

173 depths were 5, 10 and 20 cm. For sugar beet, 18 locations with measurement depths of

174 5, 20 and 50 cm were distributed in the field. Additionally, sensors were installed at three

175 locations at 3 m distance and at five locations at 11 m distance from the CRNS. For these

176 locations, the measurement depths were 5, 10 and 20 cm (JAKOBI ET AL., 2018). For

177 maize, sensors were installed at 18 locations at distances of 2, 6, 25 and 80 m from the

178 CRNS. At 2 m distance, sensors were installed at 3 locations. At the other distances,

179 sensors were installed at 5 locations. For all 18 locations, the measurement depths were

180 5, 15 and 30 cm. For this experiment, we additionally installed 12 SMT100 sensors

181 vertically at distances of < 5 m from the CRNS to determine the integral soil moisture

182 content from 0 to 10 cm depth (Figure 1) to account for the sensitivity of CRN

183　measurements to soil moisture content changes at shallow depths (FRANZ ET AL., 2012;

184　KÖHLI ET AL., 2015; SCHRÖN ET AL., 2017).

2.4. In-situ soil sampling

186　Additional hydrogen pools in the soil (θ_{off} [g/g]) modify the dependency of epithermal

187　neutrons on soil moisture content (ZREDA ET AL., 2012) and reduce the effective sensing

188　depth of CRNS (e.g., FRANZ ET AL., 2012). We determined θ_{off} alongside bulk density (ϱ_{bd}

189　[g/cm^3]) from soil samples of 30 cm length and 5 cm diameter obtained using a HUMAX

190　soil corer (Martin Bruch AG, Rothenburg, Switzerland). Soil samples were taken at all

191　SoilNet locations except for the 12 vertically inserted SMT100 sensors. For obtaining ϱ_{bd},

192　the soil cores were divided into 5 cm segments and oven-dried at 105 °C for 24 h.

193　Subsequently, the soil samples were sieved and depth-specifically mixed for each field.

194　Subsamples of 20 mg were taken from these bulk samples and heated to 1000 °C to

195　obtain θ_{off} from the weight loss using the stoichiometric ratio of oxygen to hydrogen in H_2O

196　(i.e., ~7.94). In this case, θ_{off} contains lattice water (*LW* [g/g]) and soil organic carbon

197　(*SOC* [g/g]), which are traditionally determined separately and summed (e.g., ZREDA ET

198　AL., 2012; SCHEIFFELE ET AL., 2020).

2.5. Weighting of reference measurements

200　KÖHLI ET AL. (2015) showed that the footprint of epithermal neutrons varies depending on

201　soil moisture content, air humidity, air pressure, soil bulk density and vegetation height.

202　These findings were extended for short distances (< 1 m) by SCHRÖN ET AL. (2017). In this

203　study, we used the most recent method for vertical and horizontal weighting of in-situ

204　reference soil moisture content measurements of which a brief description is given in the

205　following. For a complete description of the weighting procedure, we refer to SCHRÖN ET

206　AL. (2017).

207　For all experiments, we first obtained the vertical weights (i.e., W_d; SCHRÖN ET AL., 2017)

208　for each SoilNet location and measurement depth. Subsequently, W_d was used to derive

209　a vertically weighted soil moisture content for each location and measurement time. For

210　the vertical and horizontal weighting of in-situ ϱ_{bd} and θ_{off} measurements, we used the

211 average of the HUMAX sample depth-intervals, i.e., 2.5, 7.5, 12.5, 17.5, 22.5 and 27.5

212 cm. For maize and winter wheat, the reference soil moisture content locations were

213 determined following the radial sensitivity of CRNS. Thus, a horizontal weighting was

214 already implicitly considered. To avoid a double weighting, we first averaged the

215 measurements for each radius. Subsequently, the results for each radius were averaged

216 to obtain the vertically and horizontally weighted reference soil moisture content

217 ($\theta_{reference}$), ϱ_{bd} and θ_{off}. For sugar beet, the reference measurement were weighted using

218 the location-specific horizontal weights (i.e., W_r, SCHRÖN ET AL., 2017). At each

219 measurement time, the procedure to determine the vertical and horizontal weighting was

220 iterated four times, which was sufficient to reach convergence.

221 **2.6. Biomass measurements**

222 During the winter wheat, maize and sugar beet experiments, we sampled above- and

223 belowground biomass at eight, five and nine locations, respectively. At least four

224 measurement locations were sampled in < 20 m distance from the CRNS. At each

225 sampling location, 1 m of row was harvested, sealed air-tight, and transported to the

226 laboratory. Here, soil residues were removed and samples were split into above- and

227 belowground biomass, and subsequently weighed and oven-dried at ≤ 105 °C until a

228 constant weight was reached. Due to limited oven capacity, subsamples of ~20% of the

229 original sample weight were occasionally used. Areal average moist and dry above- and

230 belowground biomass was calculated using the arithmetic mean of all samples. As

231 suggested by FRANZ ET AL. (2013b), we assumed that the water equivalent contained in

232 biomass (*BWE* [mm]) can be approximated by the sum of the weight loss from oven-

233 drying and the stoichiometric amount of hydrogen and oxygen contained in cellulose (f_{ew},

234 ~55.6 %):

$$BWE = \left[(BM_f - BM_d) + f_{ew}\, BM_d\right]\frac{1}{p_d}\, p_w^{-1} \tag{1}$$

235 where p_w is the density of water (1000 kg/m^3), p_d is the distance between rows (m; sugar

236 beet: 0.465 m, winter wheat: 0.12 m, maize: 0.45 m) and BM_f and BM_d are the fresh and

237 dry biomass weights per 1 m of row [g], respectively. We used Equation (1) to determine

238 aboveground *BWE* (*BWE$_a$*), belowground *BWE* (*BWE$_b$*), while total *BWE* (*BWE$_{tot}$*) was
239 obtained as *BWE$_a$* + *BWE$_b$*.

240 For sugar beet and winter wheat, biomass was sampled on 11 days, respectively.
241 However, for winter wheat two of the belowground biomass samples were calculated from
242 aboveground biomass information according to BARET ET AL. (1992). For maize, the
243 observation period was only 3 months due to a drought-related emergency harvest and
244 biomass was only measured at five days. Therefore, additional *BWE* estimates were
245 obtained from bi-weekly leaf area index (*LAI*) measurements with a SS1 SunScan
246 Canopy Analysis System (Delta-T Devices, Cambridge, United Kingdom). For this, we
247 used an exponential model to relate *BWE* and *LAI* of maize:

$$BWE_{LAI} = a_1 LAI^{b1} \qquad\qquad\qquad\qquad (2)$$

248 where *a$_1$* and *b$_1$* are fitting parameters and *BWE$_{LAI}$* [mm] is the *BWE* predicted from *LAI*.
249 We fitted Equation (2) for the prediction of aboveground *BWE* (*BWE$_{a,LAI}$*) and
250 belowground *BWE* (*BWE$_{b,LAI}$*), while total *BWE* (*BWE$_{tot,LAI}$*) was obtained as *BWE$_{a,LAI}$* +
251 *BWE$_{b,LAI}$*. Linear interpolation was used to obtain *BWE* estimates at non-sampled times.

2.7. Cosmic Ray Neutron Measurements

253 We used different types of CRNS (i.e. CRS-1000, CRS-2000/B, mobile CRNS,
254 Hydroinnova LLC, Albuquerque, NM, USA) with moderated and bare detector tubes for
255 measuring epithermal and thermal neutron intensity, respectively. For more information
256 on the measurement principle, we refer to ZREDA ET AL. (2012). FERSCH ET AL. (2020)
257 provide an overview of the different detector types. We collocated several CRNS in all
258 three fields and summed up the measured neutron counts to achieve higher
259 measurement accuracy compared to a single sensor (cf. JAKOBI ET AL., 2020). In
260 particular, we operated 7 moderated and 3 bare neutron detectors in the sugar beet field,
261 8 moderated and 4 bare detectors in the winter wheat field, and 4 moderated and 3 bare
262 detectors in the maize field.

263 Before aggregation, outliers were removed from the raw neutron count time series (N_{raw})
264 of the individual detectors, irrespective of detector type, using two filtering steps. First,
265 extreme outliers were removed using two threshold values:

$$N_{c1} = \begin{cases} N_{raw} > 50\dfrac{cts}{h} \\ N_{raw} < 10\dfrac{kcts}{h} \end{cases} \tag{3}$$

266 Second, outliers relative to the 24 hours moving average (N_{c24m}) ± the Poissonian
267 uncertainty (e.g., KNOLL, 2010) associated to the 24 hours moving sum ($\sqrt{N_{c24s}}$) were
268 removed:

$$N_c = \begin{cases} N_{c1} > N_{24m} - \sqrt{N_{c24s}} \\ N_{c1} < N_{24m} + \sqrt{N_{c24s}} \end{cases} \tag{4}$$

269 Subsequently, the filtered hourly thermal (T_c) and epithermal (E_c) neutron count rates
270 were summed up.

271 The measurements of some of the thermal and epithermal detectors contained larger
272 data gaps. We obtained scaling factors (s_f) for each experiment and each detector relative
273 to the cumulative average count rate during times when all detectors of the same type
274 (i.e. T_c or E_c) were working. The s_f were used to account for missing data during
275 summation as follows:

$$\begin{aligned} E_s &= E_c \frac{1}{\sum s_f} \\ T_s &= T_c \frac{1}{\sum s_f} \end{aligned} \tag{5}$$

276 where E_s and T_s are the summed epithermal and thermal neutron count series adjusted
277 for data gaps.

278 Corrected epithermal neutron intensities (E) were obtained from E_s by applying
279 established correction procedures for variations in air pressure (DESILETS AND ZREDA,
280 2003), incoming cosmic ray neutron intensity (DESILETS AND ZREDA, 2001) and air humidity
281 (ROSOLEM ET AL., 2013). For these corrections, we used the average pressure, absolute

282   humidity and incoming cosmic ray neutron intensity measured during each of the three

283   experiments. The reference incoming cosmic ray neutron intensity was obtained from the

284   neutron monitor at Jungfraujoch (JUNG; via the NMDB neutron monitor database at

285   www.nmdb.eu). Following the experimental findings from JAKOBI ET AL. (2018), we

286   obtained the corrected thermal neutron intensity (T) from T_s by applying corrections for

287   pressure and absolute humidity only.

2.8. The thermal-to-epithermal neutron ratio

289   TIAN ET AL. (2016) found a positive correlation between BWE_a of maize and soy bean and

290   the ratio of thermal to epithermal neutrons (N_r). Such a correlation was also found for the

291   sugar beet dataset used in this study (JAKOBI ET AL., 2018). In this study, we obtained N_r

292   according to JAKOBI ET AL. (2018):

$$N_r = \frac{T}{E}\frac{\bar{E}}{\bar{T}} \tag{6}$$

293   where $\bar{E}$ and $\bar{T}$ are the arithmetic means of the epithermal and thermal neutron intensity

294   measured during each experiment, and E and T are the 12-hourly moving averages of

295   the epithermal and thermal neutron intensity. We used linear models for relating N_r and

296   BWE_a (JAKOBI ET AL., 2018):

$$BWE_{a,Nr} = a_2 Nr + b_2 \tag{7}$$

297   where $BWE_{a,Nr}$ is the BWE_a estimated from N_r and a_2 and b_2 are calibration parameters.

298   We also used a linear model for relating T and BWE_{tot}:

$$BWE_{tot,T} = a_3 T + b_3 \tag{8}$$

299   where $BWE_{tot,T}$ is the BWE_{tot} estimated from T and a_3 and b_3 are calibration parameters.

2.9. Conversion of neutrons to soil moisture content

301   We obtained volumetric soil moisture content (θ) from E with a modified approach

302   following DESILETS ET AL. (2010), which showed good performance in several previous

303   studies (e.g., RIVERA VILLARREYES ET AL., 2011; BAATZ ET AL., 2014; DONG ET AL., 2014;

304   DIMITROVA-PETROVA ET AL., 2020):

$$\theta = \varrho_{bd}\left(\frac{p_0}{\frac{fE}{N_0} - p_1} - p_2 - \theta_{off}\right) \tag{9}$$

where p_i (= 0.0808, 0.372 and 0.115) are fitting parameters obtained from neutron transport modeling, f is a temporally variable correction factor (derived from biomass measurements, N_r, or T), and N_0 is the epithermal neutron intensity above dry soil. In this study, we obtained N_0 from the 12-hourly moving average of the epithermal neutron intensity using three different strategies:

- In calibration strategy A, a single value for N_0 (i.e., $N_{0,opt}$) was obtained using the whole reference soil moisture content time series and assuming $f = 1$ (i.e. no additional correction).
- In calibration strategy B, a single value for N_0 (i.e., $N_{0,bare}$) was obtained for the first two days of the reference soil moisture content observations and assuming $f = 1$. This strategy represents the typical calibration approach using campaign-style soil sampling (e.g., ZREDA ET AL., 2012).
- In calibration strategy C, we obtained 12-hourly N_0-values using Equation (9) and assuming $f = 1$. We used the resulting N_0 time series for predicting biomass, N_r or T related effects on epithermal CRN measurements.

For calibration strategies A and B, N_0 is obtained by minimization of the root mean square error (RMSE) between the reference and the estimated soil moisture content.

2.10. Biomass, N_r and thermal neutron corrections

We tested four regression models for obtaining the correction factor f in Equation (9) using either BWE_a (e.g., BAATZ ET AL., 2015), BWE_{tot}, N_r (e.g., JAKOBI ET AL., 2018), or T:

$$N_{0,BWEa} = a_4\, BWE_a + N_{0,BWEa=0} \tag{10}$$

$$N_{0,BWEtot} = a_5\, BWE_{tot} + N_{0,BWEtot=0} \tag{11}$$

$$N_{0,Nr} = a_6\, N_r + N_{0,Nr=0} \tag{12}$$

$$N_{0,T} = a_7\, T + N_{0,T=0} \tag{13}$$

325　where a_4, a_5, a_6, and a_7 [cph] are empirical factors representing the change in N_0 per mm

326　BWE_a, mm BWE_{tot}, N_r or T, respectively and $N_{0,BWEa=0}$, $N_{0,BWEtot=0}$, $N_{0,Nr=0}$ and $N_{0,T=0}$

327　represent N_0 when BWE_a, BWE_{tot}, N_r or T, respectively equal 0. Subsequently, we derived

328　f by assuming that the changes in estimated N_0 and epithermal neutron intensity are

329　proportional:

$$f_{BWEa} = \left(1 + \frac{a_4}{N_{0,BWEa=0}} BWE_a\right)^{-1} \tag{14}$$

$$f_{BWEtot} = \left(1 + \frac{a_5}{N_{0,BWEtot=0}} BWE_{tot}\right)^{-1} \tag{15}$$

$$f_{Nr} = \left(1 + \frac{a_6}{N_{0,Nr=0}} N_r\right)^{-1} \tag{16}$$

$$f_T = \left(1 + \frac{a_7}{N_{0,T=0}} T\right)^{-1} \tag{17}$$

330　where f_{BWEa}, f_{BWEtot}, f_{Nr} and f_T are correction factors to be used with $N_{0,BWEa=0}$, $N_{0,BWEtot=0}$,

331　$N_{0,Nr=0}$ and $N_{0,T=0}$, respectively in Equation (9). We also obtained correction factors for

332　BWE_a and BWE_{tot} based on the empirical generic biomass correction model of BAATZ ET

333　AL. (2015), who found a reduction in epithermal neutron intensity of ~0.5 % per mm BWE_a:

$$f_{BWEa,Baatz} = 1 + BWE_a \frac{6.4}{1215} \tag{18}$$

$$f_{BWEtot,Baatz} = 1 + BWE_{tot} \frac{6.4}{1215} \tag{19}$$

334　where $f_{BWEa,Baatz}$ and $f_{BWEtot,Baatz}$ again are correction factors to be used in Equation (9)

335　and the constants 6.4 and 1215 [cph] are the reduction per mm BWE_a and N_0 when BWE_a

336　equals 0, respectively.

3. Results

3.1. Data Overview

339　Table 1 provides a summary of the basic soil properties for the three cropped fields. The

340　bulk density generally increased with depth for all three fields, while the additional

341　hydrogen pools θ_{off} were relatively constant with depth. It was found that the weighted

342 bulk densities were lower than the arithmetic mean due to the decreasing sensitivity of

343 CRNS with increasing depth.

Table 1: Soil bulk density (ϱ_{bd}), gravimetric soil moisture content (θ_g) and additional hydrogen pools in the soil (θ_{off}) from the HUMAX samples taken on 6 Mai 2015 for winter wheat, 6 June 2016 and 4 November 2016 for sugar beet, and 29 Mai 2018 for maize. Please note that the sugar beet soil sampling results differ in comparison to JAKOBI ET AL. (2018) and SCHEIFFELE ET AL. (2020), because the average of two sampling campaigns was used here whereas the two previous studies only used the results from the campaign on 6 June.

Depth [cm]	Winter Wheat			Sugar Beet			Maize		
	ϱ_{bd} [g/cm³]	θ_g [g/g]	θ_{off} [g/g]	ϱ_{bd} [g/cm³]	θ_g [g/g]	θ_{off} [g/g]	ϱ_{bd} [g/cm³]	θ_g [g/g]	θ_{off} [g/g]
0 – 5	1.188	0.200	0.033	1.34	0.194	0.027	1.242	0.176	0.048
5 – 10	1.262	0.197	0.032	1.396	0.189	0.027	1.256	0.192	0.049
10 – 15	1.280	0.193	0.032	1.397	0.189	0.027	1.331	0.191	0.049
15 – 20	1.274	0.190	0.032	1.375	0.187	0.028	1.344	0.196	0.049
20 – 25	1.280	0.190	0.032	1.429	0.178	0.026	1.358	0.202	0.05
25 – 30	1.284	0.122	0.032	1.464	0.170	0.026	1.288	0.198	0.048
Average	1.261	0.182	0.032	1.400	0.185	0.027	1.303	0.192	0.049
Weighted	1.247	0.192	0.023	1.379	0.189	0.016	1.277	0.186	0.034

350

Table 2: Minimum, average and maximum corrected epithermal and thermal neutron count rates measured during the experiments in sugar beet, winter wheat and maize fields.

Experiment	Corrected Epithermal Neutrons [cts/h]			Corrected Thermal Neutrons [cts/h]		
	Minimum	Average	Maximum	Minimum	Average	Maximum
Sugar Beet	8952	10425	11856	2076	2458	2786
Winter Wheat	6063	7350	8542	1296	1562	1849
Maize	4248	5273	5868	1877	2148	2499

353

354 An overview of the precipitation, normalized neutron count rates, BWE and reference soil

355 moisture content for the three cropped fields is given in Figure 2. The minimum, average

356 and maximum epithermal and thermal neutron intensity after correction are provided in

357 Table 2. Figure 2e shows that the maximum BWE_b for the three crops differed strongly.

358 Both winter wheat and maize showed relatively low maximum BWE_b values (0.89 and

359 0.85 mm, respectively), whereas the maximum BWE_b for sugar beet was tenfold higher

360   (8.23 mm). For maize, BWE_a and BWE_b were derived from LAI using Equation (2) (Figure

361   3). The high R^2 (≥ 0.95) indicates that LAI was a good predictor for BWE_a and BWE_b.

362   Therefore, we used the LAI-derived BWE of maize in the remainder of the manuscript.
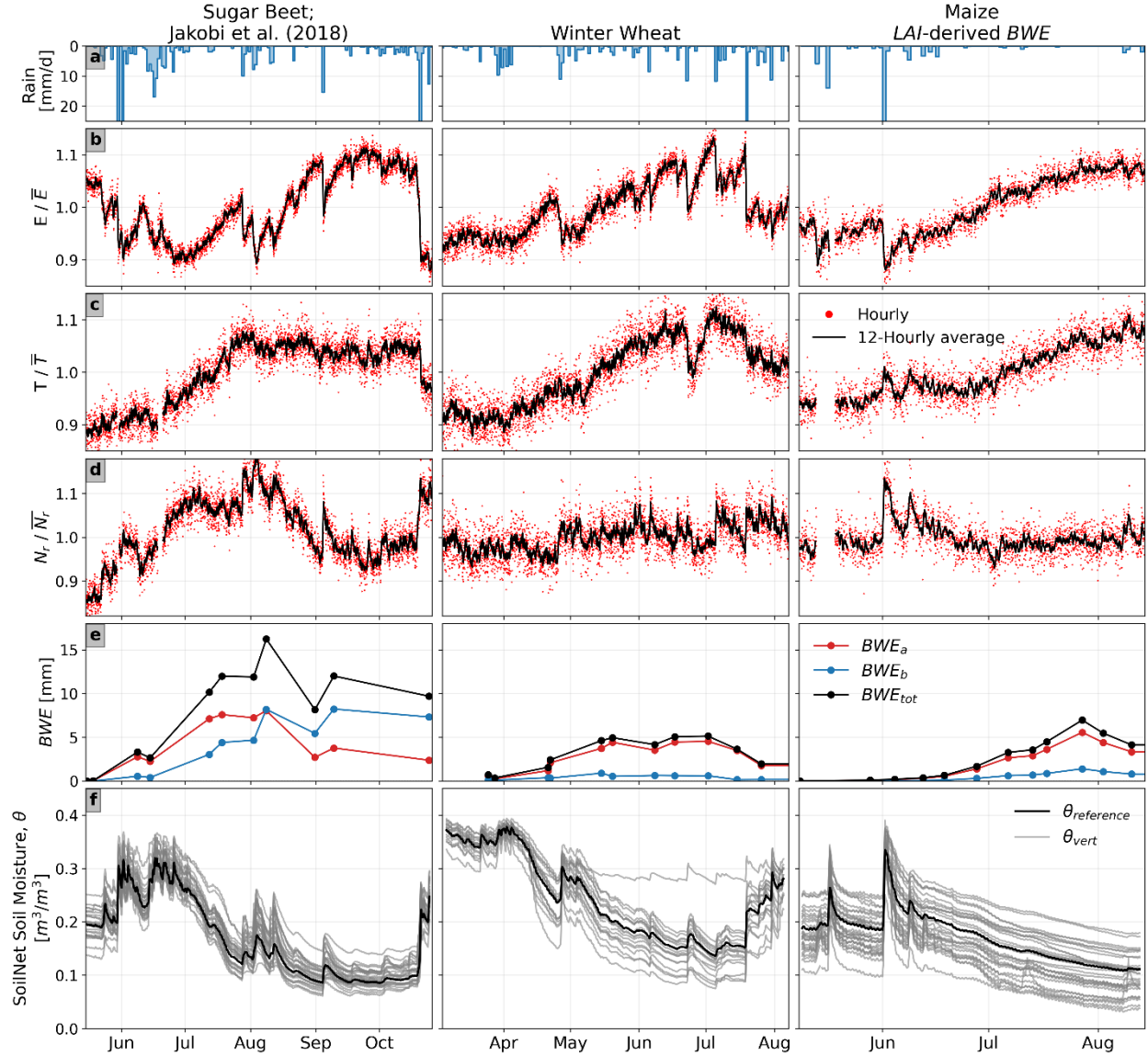

363
364   *Figure 2: Time series of a) precipitation, b) epithermal neutron intensity (E) normalized by the average E,*
365   *c) thermal neutron intensity (T) normalized by the average T, d) neutron ratio (N_r), e) aboveground,*
366   *belowground and total biomass water equivalent (BWE_a, BWE_b and BWE_{tot}, respectively) and f) soil*
367   *moisture content obtained from the vertically and horizontally weighted SoilNet measurements (black,*
368   *$\theta_{reference}$) and the vertically weighted SoilNet measurements (grey, θ_{vert}).*

369   Figure 2f shows the vertically weighted soil moisture content measured at all SoilNet

370   locations as well as the horizontally and vertically weighted reference soil moisture

371   content for the three crops. The average reference soil moisture content for sugar beet

372 and maize was notably lower (~0.17 m³/m³) compared to winter wheat (0.24 m³/m³) due
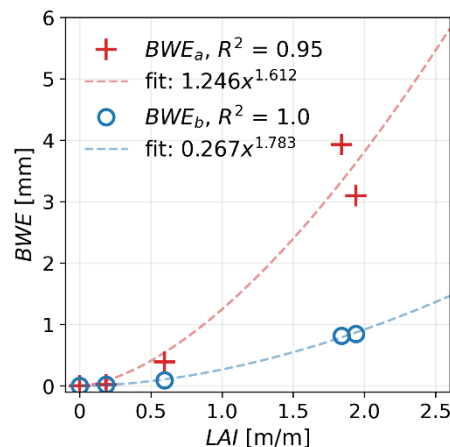373 to the drought conditions in 2016 and 2018.

374

Figure 3: Relationship between leaf area index (LAI) and above- and belowground biomass water equivalent (BWE$_a$ and BWE$_b$, respectively) for maize. The coefficients of determination (R^2) and the exponential models for predicting BWE from LAI are also provided.

3.2. The effect of time-variable biomass on CRNS derived soil moisture content

379 To investigate the influence of vegetation biomass on soil moisture content estimates with
380 CRNS, we first calibrated N_0 during bare soil condition (calibration strategy B, Figure 4c,
381 red). For all three crops, the soil moisture content estimated from the CRN measurements
382 in this way deviated from the reference soil moisture content. This was attributed to
383 increasing biomass associated with crop growth (Figure 4c, red areas) and resulted in a
384 high RMSE of 0.097 m³/m³ for sugar beet, 0.041 m³/m³ for winter wheat and 0.019 m³/m³
385 for maize. For sugar beet and winter wheat, the CRNS mostly overestimated soil moisture
386 content, indicating that the additional hydrogen in the biomass decreased the local
387 epithermal neutron intensity. This effect was particularly strong in case of sugar beet due
388 to its higher above- and belowground biomass. Interestingly, CRNS mostly
389 underestimated soil moisture content for maize, even though the progressing growth of
390 maize should have resulted in more neutron moderation (i.e. soil moisture content
391 overestimation). This counterintuitive result can be explained by the fact that the atomic
392 nuclei of the high-growing maize surrounding the CRNS acted as scattering centers that
393 effectively increased the neutron travel paths and thus the local epithermal neutron

394   intensity (LI ET AL., 2019). In contrast to maize, winter wheat and sugar beet did not grow

395   high enough in the near field of the detector, so this effect was not observed.

396   Figure 4c also shows the results of calibration strategy A, which considers all reference

397   soil moisture content data but no time-variable changes in biomass. For maize and winter

398   wheat, the reference and CRNS derived soil moisture content showed good agreement

399   and the RMSE was relatively low (i.e., 0.031 m^3/m^3 for winter wheat and 0.011 m^3/m^3 for

400   maize). For sugar beet, the visual agreement was not as good, and this was supported

401   by the higher RMSE (0.042 m^3/m^3).

402
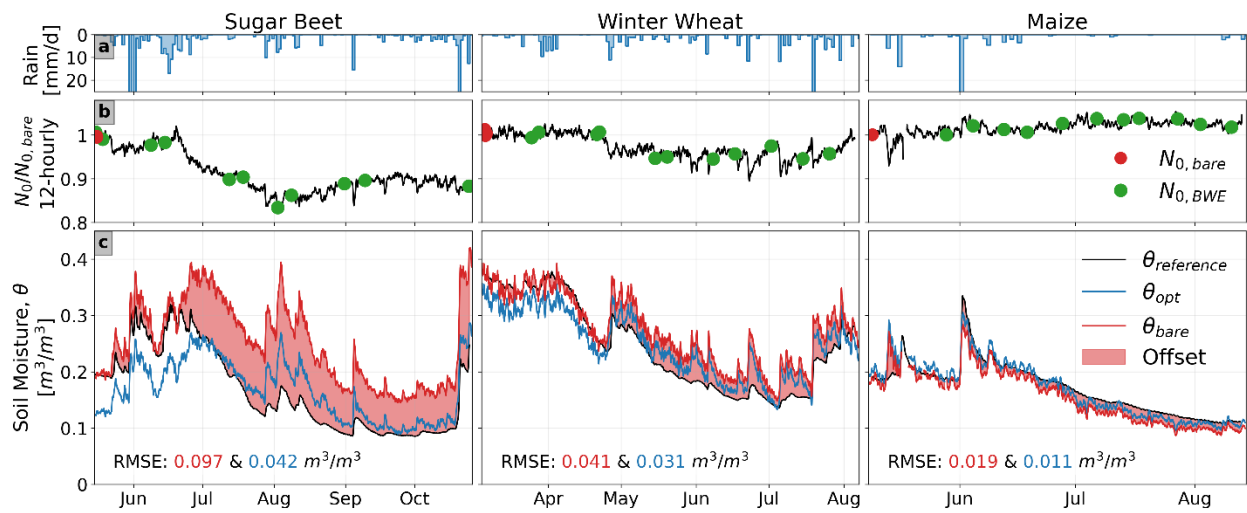
Figure 4: Time series of a) precipitation b) N_0 at biomass sampling dates and c) offset between reference
soil moisture content and CRNS derived soil moisture content using strategy B (i.e. bare soil calibration).
CRNS derived soil moisture content using strategy A (in blue), i.e., by optimising the entire time series of
reference soil moisture content, is also shown.

3.3. Soil moisture content correction with local biomass measurements

408   To quantify the effect of biomass on soil moisture content obtained with CRNS, we

409   established linear regression models between the in-situ measured BWE_a and BWE_{tot}

410   and the calibration parameter N_0 (Figure 5). We found distinct differences in the $N_0 - BWE$

411   relationships for the three crops. For sugar beet and winter wheat, N_0 showed a negative

412   relationship with BWE, whereas for maize this relationship was positive for reasons

413   already provided. For sugar beet, the slopes of the $N_0 - BWE_a$ and $N_0 - BWE_{tot}$

414   relationships differed more strongly compared to the other crops (Figure 5a), which can

415   be explained by the higher amount of belowground biomass compared to maize and

416 winter wheat (see also Figure 2e). In addition, the $N_0 – BWE_{tot}$ relationship for sugar beet
417 resulted in a higher R^2-value compared to the $N_0 – BWE_a$ relationship, indicating that the
418 total biomass should be preferably used for correction in case of sugar beet. Figure 5 also
419 shows that the relationship suggested by BAATZ ET AL., 2015 (i.e. a reduction of ~0.5 % of
420 N_0 per mm BWE_a) was not able to represent the influence of biomass on N_0, except to
421 some extent for winter wheat.

422
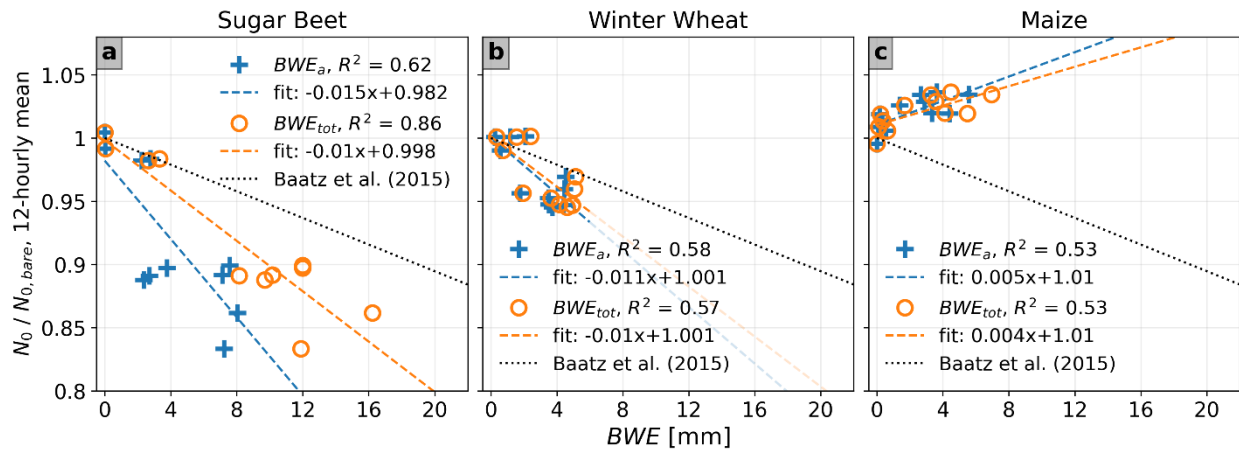
Figure 5: Scatterplots and corresponding linear regressions for predicting the change in N_0 from BWE_a (blue) and BWE_{tot} (orange), respectively. The slopes of all linear fits were significantly different from 0 (i.e., the two-sided p-value was < 0.05 for a test with the null hypothesis that the slope is equal to zero). Additionally, the empirical model from BAATZ ET AL. (2015) for predicting the change in N_0 from BWE_a is shown.

428 In a next step, the BWE_a and BWE_{tot} regression models were used for the correction of
429 CRNS soil moisture content using Equations (14) and (15). Figure 6 shows that these
430 corrections were able to effectively reduce the biomass effects for all three crops. In case
431 of winter wheat and maize, a correction based on BWE_a was sufficient to obtain a low
432 RMSE (0.018 and 0.009 m^3/m^3, respectively). In the case of sugar beet, a correction
433 based on BWE_{tot} led to a substantially lower RMSE of 0.015 m^3/m^3 compared to 0.032
434 m^3/m^3 when only BWE_a was considered.

435 For winter wheat, the relationship of BAATZ ET AL. (2015) showed an acceptable
436 performance in terms of RMSE in comparison to the linear regression models (Figure 6).
437 For sugar beet, the RMSE considering biomass correction with the relationship of BAATZ
438 ET AL. (2015) increased CRNS accuracy compared to the worst-case calibration (i.e.
439 strategy B), but was much higher in comparison to the linear regression models (Figure

6), even when BWE_{tot} (Equation (19), RMSE of 0.048 m³/m³) was used instead of BWE_a (Equation (18), RMSE of 0.071 m³/m³). As the empirical correction proposed by BAATZ ET AL. (2015) greatly relies on forest biomass data, it implicitly considers a root-shoot ratio valid for trees (i.e., in the order of ~0.2 – 0.6; MOKANY ET AL., 2006). In contrast, the root-shoot ratio of crops changes with time. Sugar beet, for example, showed an increase from ~0.2 to ~6 for the root-shoot ratio. Therefore, the root biomass is not adequately represented by the relationship of BAATZ ET AL. (2015). For maize, the relationship of BAATZ ET AL. (2015) resulted in a decreased accuracy due to the additional neutron scattering processes discussed earlier.
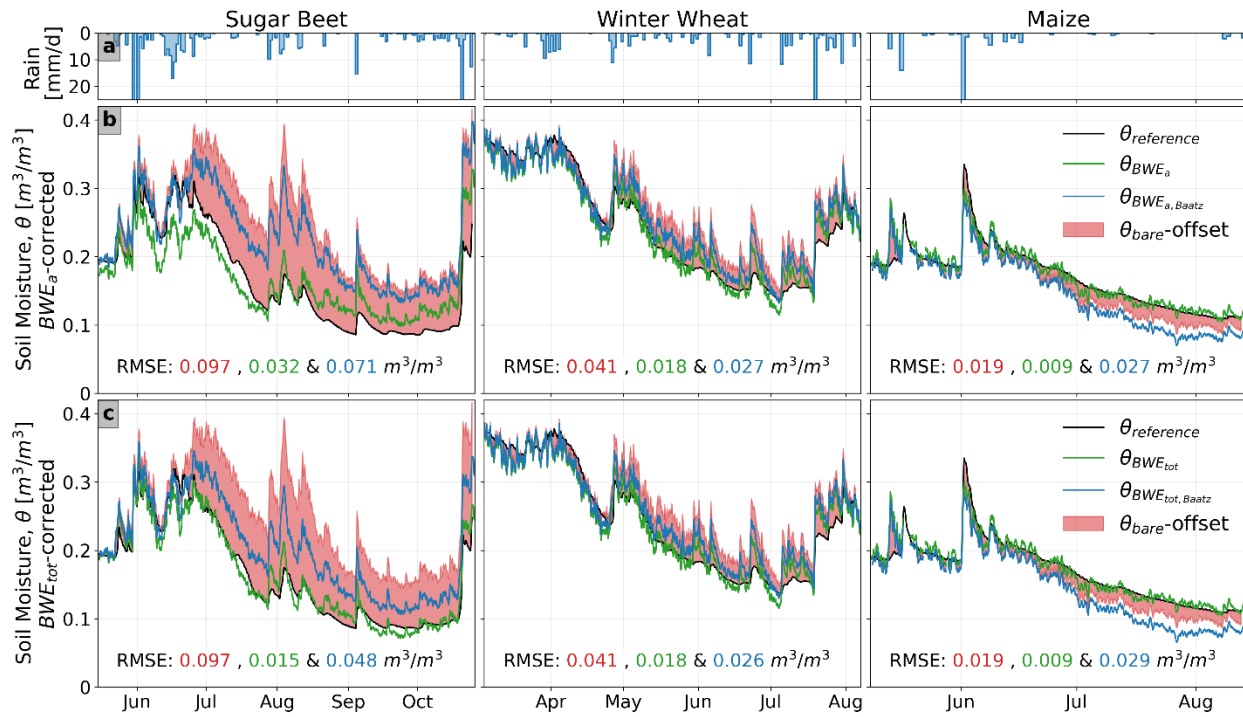
Figure 6: Times series of a) precipitation, b) CRNS derived soil moisture content corrected for aboveground biomass and c) CRNS derived soil moisture content corrected for total biomass. For the biomass correction, local linear regression models (green) and the empirical approach from BAATZ ET AL. (2015) (blue) were considered. For comparison, the vertically and horizontally weighted reference soil moisture content (black) and the offset due to the bare soil calibration (red) are shown.

3.4. Soil moisture content correction with the neutron ratio

We also investigated the possibility of using N_r for the correction of CRNS derived soil moisture content (TIAN ET AL., 2016; JAKOBI ET AL., 2018; VATHER ET AL., 2020). For this, we established linear regression models between N_0 and N_r (Figure 7) using all

measurements from the observation period (Figure 7, black) and measurements on biomass measurement dates only (Figure 7, orange). For sugar beet (JAKOBI ET AL., 2018) and winter wheat, linear relationships between N_r and N_0 were found when considering the whole measurement period (Figure 7a and Figure 7b). For maize, a much flatter regression slope was found (Figure 7c) and the R^2 was also lower (0.06) compared to sugar beet (0.44) and winter wheat (0.52). If only days with in-situ BWE samples were considered, the R^2 for sugar beet (0.77) and winter wheat (0.70) increased, while the R^2 for maize decreased to 0.03. Except for maize with in-situ biomass sample times only, all slopes were significantly different from 0 ($p < 0.05$).
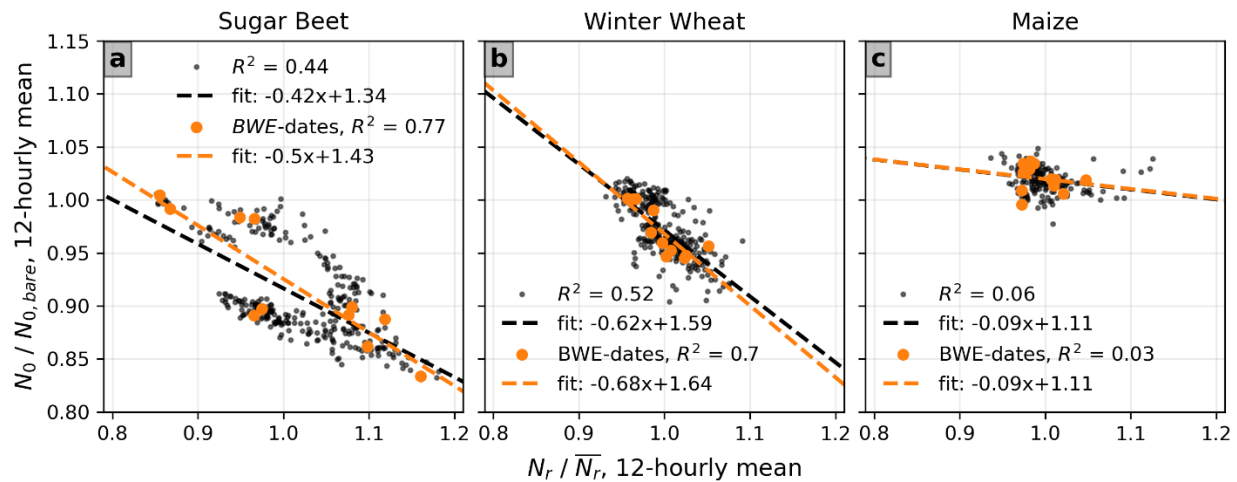

Figure 7: Relationships between normalized N_r and normalized N_0. Additionally, the relationships when using the biomass sampling dates (orange) only are shown. Except for the relationship for maize considering only the times of BWE measurements, all linear regressions have slopes that are significantly different from 0 (i.e., the two sided p-value was < 0.05 for tests with the null hypothesis that the slopes are equal to zero).

The linear regression models for predicting N_0 from N_r were also used for the correction of soil moisture content estimates using Equation (16) (Figure 8). For all three crop types, the soil moisture content estimates obtained using a correction based on N_r were more accurate than the estimates obtained using calibration strategy B as indicated by the lower RMSE of 0.032, 0.022 and 0.011 m^3/m^3 for sugar beet, winter wheat and maize, respectively. If only N_r values at times of biomass measurements were used to derive the

480 correction models (Figure 7, orange), similar results were obtained except for maize due
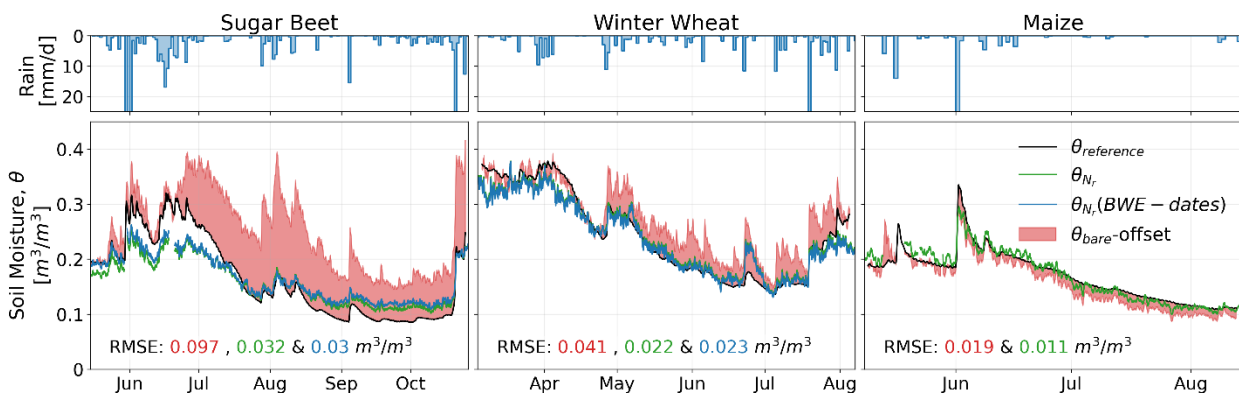481 to the insignificant regression model (Figure 7c).

482

483 *Figure 8: Times series of the CRNS derived soil moisture content corrected with Nr (green) and Nr obtained*
484 *during times of biomass sampling (blue). For comparison, the vertically and horizontally weighted*
485 *reference soil moisture content (black) and the offset resulting from bare soil calibration of the CRNS (red)*
486 *are also shown.*

3.5. Soil moisture content correction with thermal neutrons

488 In a next step, we investigated the possibility of using the thermal neutron intensity for the
489 correction of biomass effects on soil moisture content estimation with CRNS. For this, we
490 established linear regression models for predicting the change in the calibration
491 parameter N_0 from the thermal neutron intensity using all measurements from the
492 observation periods (Figure 9, black) and measurements from the biomass measurement
493 dates only (Figure 9, orange). All three crop types showed linear $T - N_0$ relationships like
494 the relationships between BWE_{tot} and N_0 (Figure 5), with sugar beet showing the steepest
495 regression slope and maize showing a positive relationship between T and N_0. When only
496 the biomass measurement dates were used, higher correlations were obtained (Figure
497 9a-c). However, the regression results were similar to the case where all data were
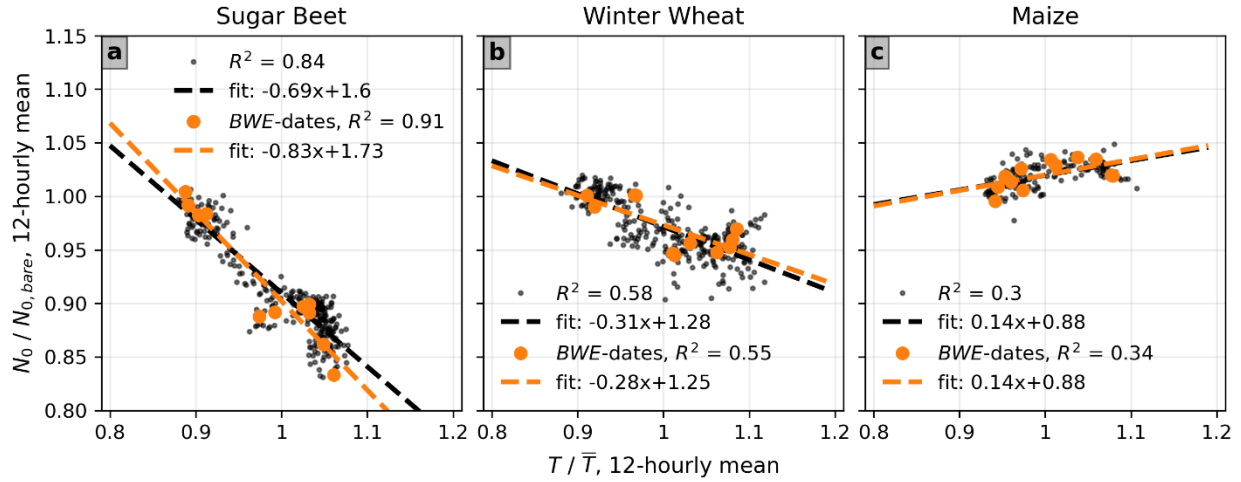498 considered.

499

Figure 9: Relationship between normalized thermal neutron intensity and normalized N_0 for (a) sugar beet, (b) winter wheat, and (c) maize (black). Additionally, the relationships if only observations at dates of biomass water equivalent (BWE) sampling (orange) were considered are shown. The slopes of all regression models were significantly different from 0 (i.e., the two sided p-value was < 0.05 for tests with the null hypothesis that the slopes are equal to zero).

Subsequently, the linear regression models for predicting the change in N_0 from the thermal neutron intensity were used for correcting CRNS soil moisture content estimates using Equation (17) (Figure 10). For all three crop types, the correction using thermal neutrons produced better results than the calibration strategy B as indicated by the decrease in RMSE to 0.017, 0.019 and 0.009 m³/m³ for sugar beet, winter wheat and maize, respectively. The results were similar when the linear regression models based only on days with biomass measurements were considered (Figure 9, orange).
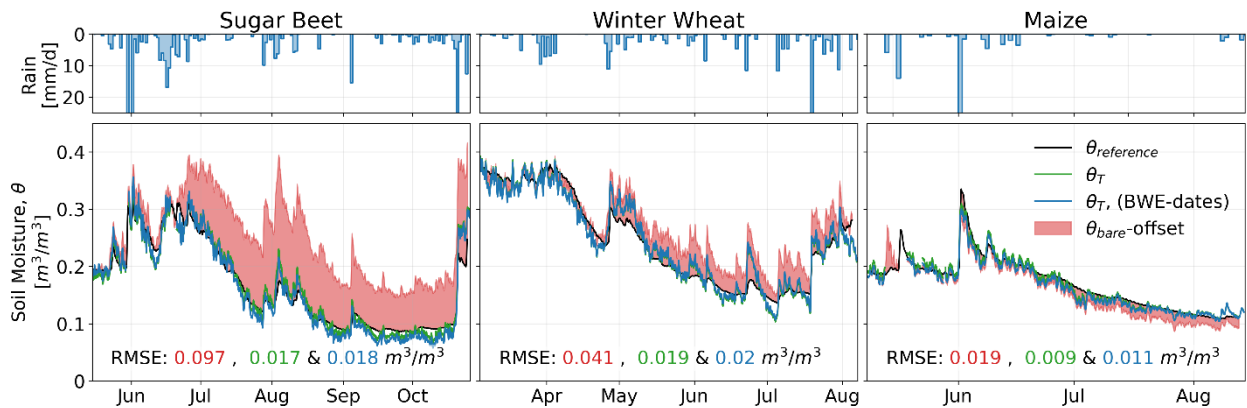

512

Figure 10: Times series of the CRNS derived soil moisture content corrected with thermal neutrons (green) and with thermal neutrons obtained during dates of biomass sampling (blue). For comparison, the vertically and horizontally weighted reference soil moisture content (black) and the offset obtained from bare soil calibration (red) are shown.

3.6. Biomass estimation from the neutron ratio

After evaluating different approaches for correcting soil moisture content estimates, we now evaluate the potential of N_r for estimating crop biomass development (TIAN ET AL., 2016; ANDREASEN ET AL., 2017a; JAKOBI ET AL., 2018). The N_r for sugar beet was linearly correlated with in-situ measured BWE_a (Figure 11a; JAKOBI ET AL., 2018). In contrast, the linear regressions for winter wheat and maize did not indicate significant slopes (i.e., the two-sided p values for a test with the null hypothesis that the slopes are equal to zero were > 0.05, Figure 11b and Figure 11c). This means that the prediction of aboveground biomass from N_r was not possible for winter wheat and maize in our study. TIAN ET AL. (2016) and VATHER ET AL. (2020) suggested to use uncorrected thermal and epithermal neutron intensities for the derivation of the N_r. However, this reduced the R^2 of the N_r - BWE_a relationship from 0.12 to 0.00 for winter wheat and from 0.92 to 0.73 for sugar beet, while it increased R^2 only slightly for maize (from 0.02 to 0.04). It has to be noted that an outlier was removed for sugar beet (Figure 11a, circle with dot; also see Jakobi et al., 2018). If this measurement was included in the analysis, the R^2 was reduced to 0.68.

Because N_r could also be influenced by changes in soil moisture content, we also investigated the N_r – soil moisture content relationship. However, we found only weak relationships for all three crops that could not be well described with linear or exponential models (Figure 11d – Figure 11f). For winter wheat and maize, the slopes of the linear regressions were significantly different from 0 (i.e., two-sided p < 0.05, Figure 11e and Figure 11f). However, the low R^2-values (≤ 0.34) indicated only weak dependencies. For sugar beet, the R^2 was 0.00. These results confirm previous findings by TIAN ET AL. (2016) and ANDREASEN ET AL. (2017a) that the N_r is only weakly related to soil moisture content.

We observed hysteretic behavior in the soil moisture content - N_r relationship for sugar beet (Figure 11d). Similarly, the N_r – N_0 relationship also showed hysteresis (Figure 7a). The color sequence showing the development of BWE_{tot} (Figure 11d) indicates that the hysteresis could be related to sugar beet growth, which is also characterized by changes in plant structure (e.g. development of leaves and tap roots; see also Appendix A). However, the hysteresis could also be an effect of the soil (and plant) heterogeneity in field F01 (shown in Figure 1 in JAKOBI ET AL., 2018), which may affect thermal and

547 epithermal neutron intensities differently due to the different radial footprints. We also
548 tested if BWE_b or BWE_{tot} for sugar beet could be predicted from N_r, but found lower R^2
549 values (0.35 and 0.73, respectively) in comparison to the R^2 calculated between N_r and
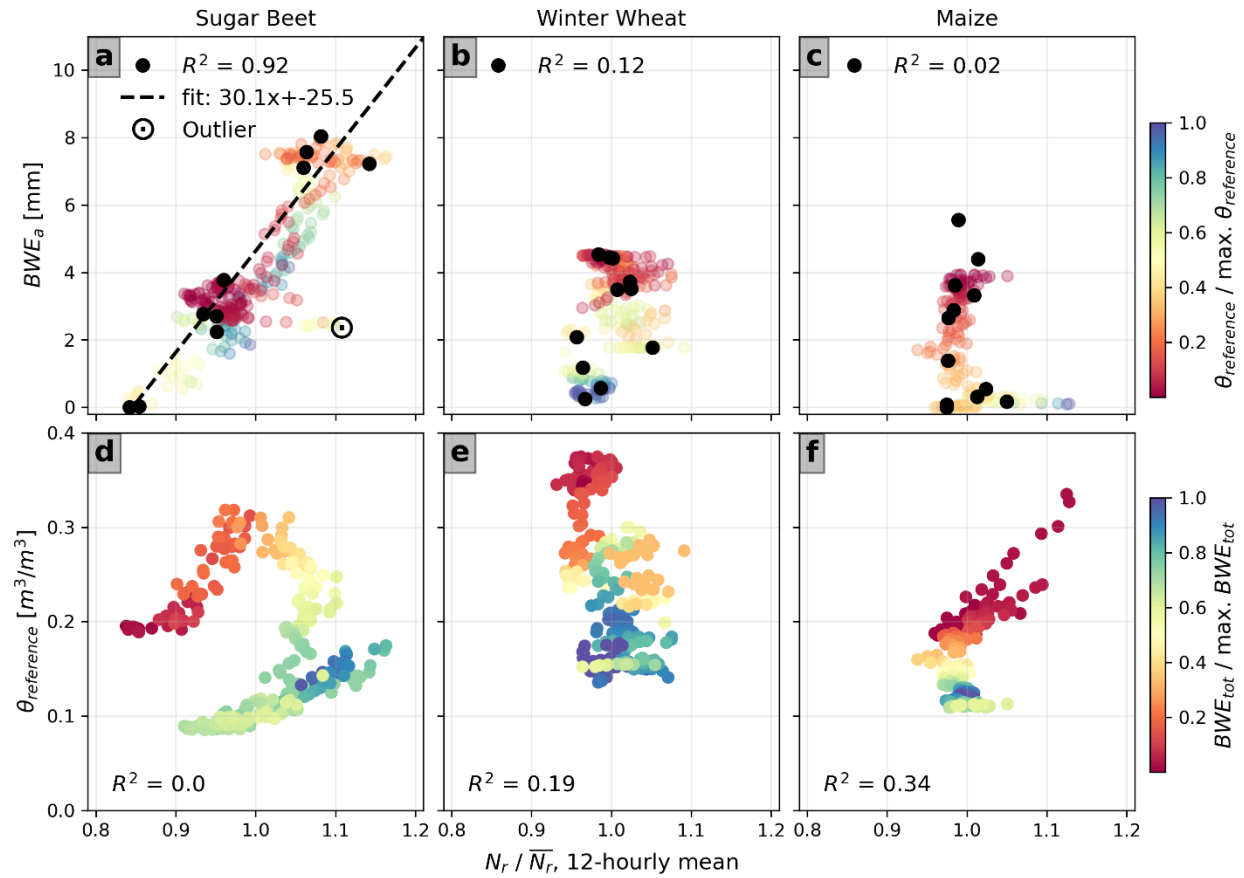550 BWE_a (0.92, Figure 11a).

551

Figure 11: Relationships of neutron ratio (N_r) normalized with the average N_r of the whole time series and measured aboveground biomass water equivalent (BWE_a) of (a) sugar beet, (b) winter wheat, and (c) and maize and relationships of N_r with horizontally and vertically weighted reference soil moisture content ($\theta_{reference}$) for (d) sugar beet, (e) winter wheat, and (f) maize, respectively. The colouring sequences in subplots a) – c) indicate changes in $\theta_{reference}$. The colouring sequences in subplots c) – f) indicate changes in BWE_{tot} (linearly interpolated). Additionally, the linear regression model for deriving BWE_a from N_r for the Sugar Beet experiment is shown. The slopes of the linear regressions were significantly different from 0 for the relationships presented in subplots a), e) and f) (i.e., the two-sided p-value was < 0.05 for a test with the null hypothesis that the slope is equal to zero).

3.7. Biomass estimation from thermal neutrons

562 Finally, we investigated the potential of T for estimating biomass of the considered crops
563 (Figure 12a - Figure 12c). For all three crop types, T was linearly related with in-situ

564 measured BWE_{tot}. R^2 was lowest for winter wheat (0.69), while it was 0.87 for sugar beet
565 and maize. The steepest regression slope was obtained for sugar beet, while the slopes
566 for maize and especially for winter wheat were much lower. For sugar beet, the R^2 was
567 slightly lower compared to the R^2 that was found for predicting BWE_a from N_r. For winter
568 wheat, the relatively low R^2 may be related to the large equipment island, where only a
569 thin grass cover was present and no crops were growing. Thus, soil moisture content may
570 have been of greater importance for the thermal neutron intensity in the case of winter
571 wheat as compared to sugar beet and maize.

572 The scatter plots (Figure 12d–f) suggest that the thermal neutron intensity is influenced
573 by soil moisture content, which seems to contradict our findings above. However, this
574 apparent dependence of thermal neutron intensity on soil moisture content can be
575 explained by the fact that for our experiments the increase of biomass usually coincides
576 with decreasing soil water content due to increasing water demand of the crops (see
577 Figure 2e and Figure 2f). In addition, there are also periods where the thermal neutron
578 intensity stayed almost constant during bare field conditions, while the reference soil
579 moisture content increased considerably (Figure 12d and Figure 12f) indicating that
580 thermal neutron intensity was independent of soil moisture content.

581 Since all relationships were significant, the linear regression models from Figure 12a–c
582 were used for estimating temporally variable BWE_{tot} for all three crop types (Figure 13).
583 The RMSE indicated an estimation accuracy of 1.92, 0.97 and 0.98 mm for sugar beet,
584 winter wheat and maize, respectively, which corresponded to 22, 33 and 42 % of the
585 average interpolated BWE_{tot}. Larger deviations were mostly associated with precipitation
586 events, which sometimes resulted in a decrease of the thermal neutron intensity and thus
587 underestimated BWE_{tot} (e.g. at the end of the measurement period of sugar beet). In other
588 periods, the thermal neutron intensity and thus BWE_{tot} increased with precipitation (e.g.
589 beginning of June for maize). For winter wheat, BWE_{tot} was systematically
590 underestimated from the end of April until the beginning of June and overestimated from
591 the beginning of July until the end of the observation period (Figure 13). These deviations
592 can also be identified in Figure 12b (with $T \sim 1$ and $BWE \sim 2 - 4$ mm) and can possibly be
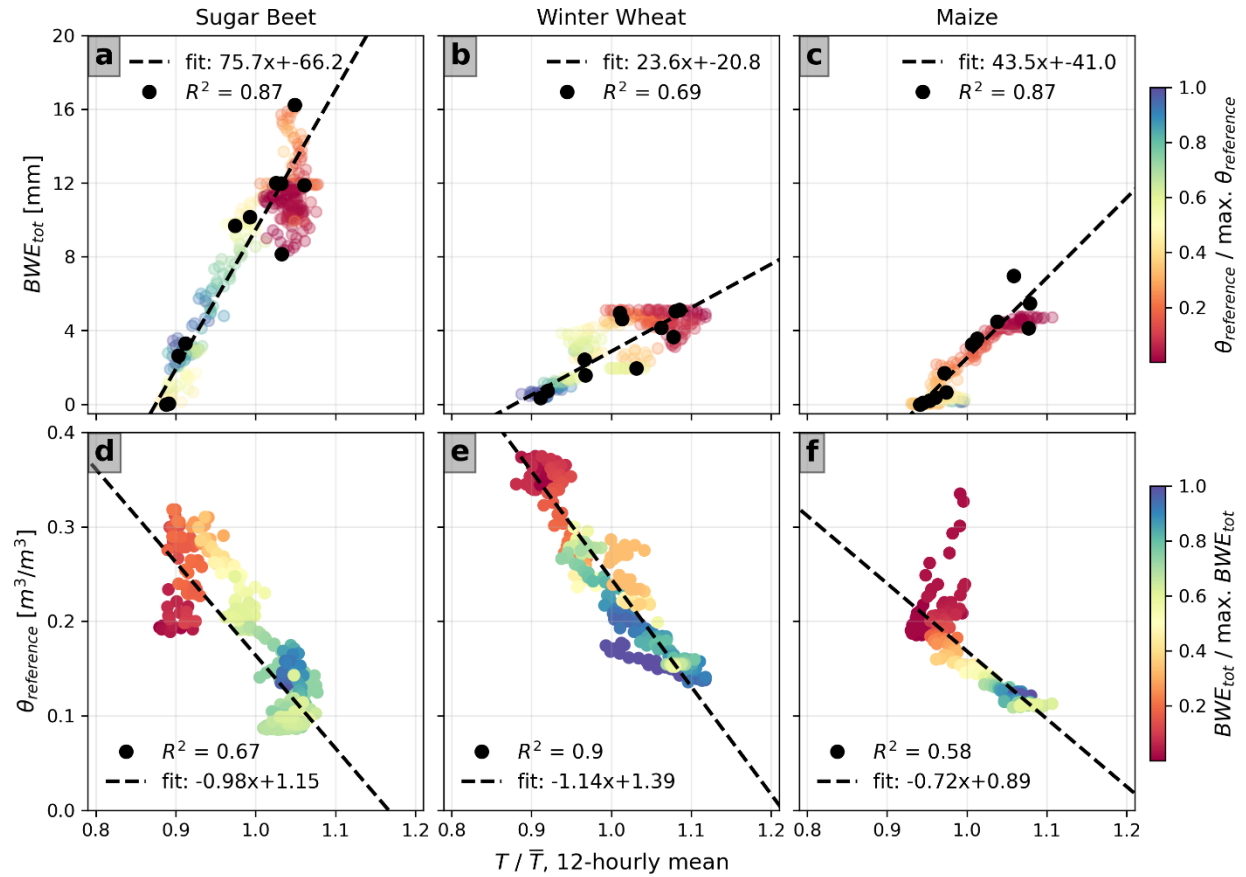593 explained with a change in plant structure in the growing season.

594

Figure 12: Scatter plots of normalized thermal neutron intensity (T) and BWE_{tot} as well as T and the reference soil moisture content ($\theta_{reference}$) for (a, d) sugar beet, (b, e) winter wheat, and (c, f) maize. The colouring sequence in subplots a) – c) indicate changes in $\theta_{reference}$. The colouring sequence in subplots c) – f) indicate changes in BWE_{tot} (linearly interpolated). All linear regressions have slopes that are significantly different from 0 (i.e., the two sided p-value was < 0.05 for tests with the null hypothesis that the slopes are equal to zero).
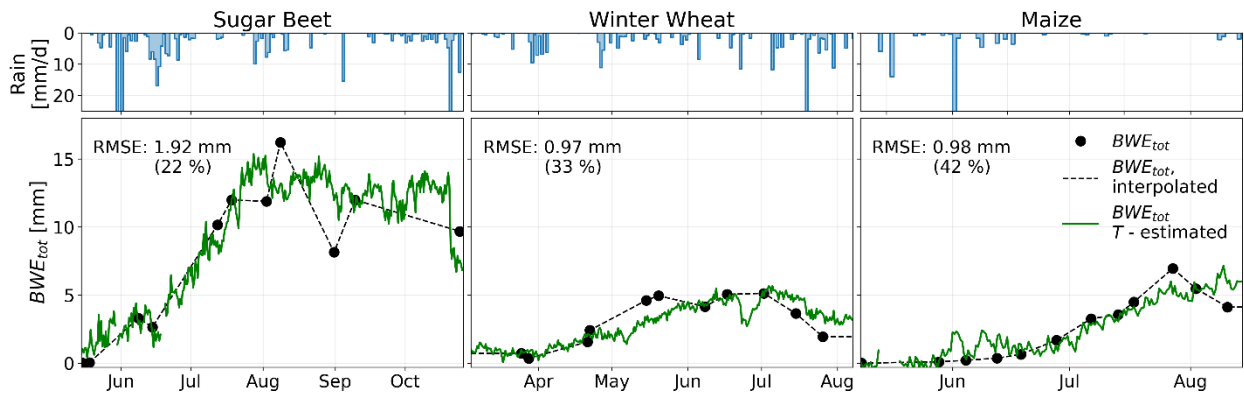

601

Figure 13: Time series of precipitation and the measured (black dots), interpolated (striped lines) and thermal neutron (T) estimated (green lines) sum of the above- and belowground biomass water equivalent (BWE_{tot}) for sugar beet, winter wheat and maize. Furthermore, the root mean square error (RMSE) and the RMSE relative to the average interpolated BWE_{tot} are provided.

4. Discussion

4.1. Correction of biomass effects on soil moisture content estimates with CRNS

The strategies for correcting soil moisture content estimates with CRNS for biomass effects, the associated measurement requirements, and the resulting RMSE are summarized in Table 3. We found that correcting the epithermal neutron intensities based on local linear regression models between N_0 and BWE, N_r or the thermal neutron intensity led to improved performance compared to the widely used bare soil calibration (e.g., ZREDA ET AL., 2012; BAATZ ET AL., 2014; HAWDON ET AL., 2014; BOGENA ET AL., 2018; COOPER ET AL., 2021). Considering in-situ measured BWE_{tot} always resulted in the most accurate CRNS based soil moisture content estimates, but this requires several reference soil moisture content and biomass measurements during the growing season. The second highest accuracy was achieved when thermal neutron intensity was used for correction (see Table 3). This correction approach only requires thermal neutron and soil moisture content measurements. Even though N_r was insensitive to biomass changes of winter wheat and maize in this study, the accuracy achieved using a correction based on N_r was similar to the accuracy achieved with in-situ measured aboveground biomass with the added advantage that no in-situ biomass information is required (see Table 3; TIAN ET AL., 2016; JAKOBI ET AL., 2018; VATHER ET AL., 2020). The empirical relation of BAATZ ET AL. (2015) also resulted in a considerable improvement in accuracy for sugar beet and winter wheat, and the performance could possibly be improved if an exponential instead of a linear model would be considered (e.g., HAWDON ET AL., 2014). However, the relation of BAATZ ET AL. (2015) failed to represent the effect of maize biomass on the epithermal neutron intensity, because of the observed increase in N_0 with increasing biomass (see Figure 5). Nevertheless, considering the biomass effect on CRNS based soil moisture content estimates through this type of generic empirical model is still appealing because it only requires biomass estimates and no soil moisture content measurements are required (Table 3; HAWDON ET AL., 2014; BAATZ ET AL., 2015).

Table 3: Calibration/correction strategies, measurement requirements and associated root mean square error (RMSE) of the CRNS derived soil moisture content estimations for the three crops. Green and orange highlight the best and second-best performance, respectively, and red highlights the worst performance in RMSE.

Calibration/Correction strategy	Measurement Requirements (in addition to epithermal CRN measurements)	Sugar Beet	Winter Wheat	Maize
		RMSE [m³/m³]		
Optimized (no correction, strategy a)	Multiple in-situ soil moisture contents (here continuous measurements)	0.042	0.031	0.011
Bare soil (no correction, strategy b)	One in-situ soil moisture content in the beginning of the measurement	0.097	0.041	0.019
BWE$_a$	Multiple aboveground biomasses and in-situ soil moisture contents measured at the same time	0.032	0.018	0.009
BWE$_{tot}$	Multiple total biomasses and in-situ soil moisture contents measured at the same time	0.015	0.018	0.009
BWE$_{a, Baatz}$	One in-situ soil moisture content with low aboveground biomass and multiple aboveground biomasses	0.071	0.027	0.027
BWE$_{tot, Baatz}$	One in-situ soil moisture content with low total biomass and multiple total biomasses	0.048	0.026	0.029
N_r (N_r at BWE-dates)	Multiple in-situ soil moisture contents and thermal neutron detectors	0.032 (0.03)	0.022 (0.023)	0.011 (-)
T (T at BWE-dates)	Multiple in-situ soil moisture contents and thermal neutron detectors	0.017 (0.018)	0.019 (0.02)	0.009 (0.011)

The improved accuracy of the soil moisture content estimates after correction using the thermal neutron intensity or N_r may potentially also be explained by the shallower penetration depth of thermal neutrons (JAKOBI ET AL., 2021) compared to epithermal neutrons (FRANZ ET AL., 2012; KÖHLI ET AL., 2015; SCHRÖN ET AL., 2017). It is possible that the corrections considering thermal neutrons (i.e., also N_r) compensate for the vertical soil moisture content heterogeneity. To this end, reference soil moisture content information in depths < 5 cm was not available in our experiments and thus not considered in the vertical weighting function for epithermal neutrons of SCHRÖN ET AL. (2017). This would be consistent with earlier studies that reported the strong influence of vertical soil moisture content heterogeneity on the accuracy of soil moisture content estimation from epithermal neutrons (FRANZ ET AL., 2013a; BARONI ET AL., 2018; SCHEIFFELE ET AL., 2020) and suggested to additionally install point sensors for estimating a field-representative shape of the soil moisture content profile (SIGOUIN ET AL., 2016; BARONI ET AL., 2018; SCHEIFFELE ET AL., 2020).

4.2. Biomass estimation with CRNS

The experiments with three crop types showed that N_r cannot generally be used for the prediction of aboveground biomass, as suggested in earlier studies (TIAN ET AL., 2016; ANDREASEN ET AL., 2017a; JAKOBI ET AL., 2018; VATHER ET AL., 2020). The estimation of aboveground biomass from N_r was possible for sugar beet, but not for winter wheat and maize in this study (Figure 11). In contrast, the estimation of total biomass (above- and belowground biomass) from thermal neutron intensity alone was possible for all investigated crops. However, the empirical relationships between thermal neutron intensity and biomass varied considerably between the three crops (Figure 12a-c). A possible explanation for this could be a variation in soil chemistry that affected the intensity of the thermal neutrons differently for the three investigated fields (ZREDA ET AL., 2008). However, this is unlikely as the three fields are very close to each other and with the same geology, so that the differences in soil chemistry are only marginal. Therefore, we assume that the relationship between the thermal neutron intensity and biomass is mainly plant-specific, i.e. influenced by plant structure.

Furthermore, we found that the observed correlation between thermal neutron intensity and soil moisture content (Figure 12d-f) is only apparent due to the simultaneous development of biomass. This finding is supported by the study of TIAN ET AL. (2016) in which thermal neutron intensity also increased mainly with increasing biomass (see Figure 4 in TIAN ET AL., 2016). Since snow is expected to affect thermal neutron intensity in a similar way as vegetation cover, our interpretations are also supported by findings from DESILETS ET AL. (2010). They showed that the thermal neutron intensity increased strongly with the onset of snow precipitation, while the epithermal neutron intensity decreased. This finding was verified using neutron transport simulations, where a ~2.5 fold increase in thermal neutron intensity for increasing snow thickness up to ~3 g/cm^2 was found as compared to snow free conditions (see Figure 4 in ZWECK ET AL., 2013). In contrast, the reduction in thermal neutron intensity due to increasing soil moisture content from ~0.10 – 0.45 m^3/m^3 can be approximated from neutron transport simulations presented in Figure 2 of ZREDA ET AL. (2008) and is expected to amount up to ~20 % only, depending on soil chemistry. Consequently, the thermal neutron intensity should be

682   affected more strongly by crop biomass than soil moisture content, thus opening the
683   possibility of biomass estimation from thermal neutron intensity as shown in our study.

4.3. Vegetation influence on neutron intensities

685   Figure 14 summarizes important vegetation-related processes controlling the epithermal
686   and thermal neutron intensity. In case of bare soil conditions (Figure 14a), thermal
687   neutrons are mainly produced in the ground. In case vegetation is present, the epithermal
688   neutron intensity is decreased by moderation of biomass, resulting in additional
689   production of thermal neutrons (Figure 14c). Moreover, in case large amounts of
690   belowground biomass are present (e.g., as for sugar beet), thermal neutron production in
691   the ground is additionally enhanced (Figure 14b). When the detector is surrounded by tall
692   vegetation (e.g., as for maize), the greater density of scattering centers (i.e., atomic nuclei
693   of the biomass) increases the local neutron density, resulting in a higher neutron detection
694   probability (LI ET AL., 2019). This phenomenon was observed for maize in this study
695   (Figure 5c), but not for the other crops. This indicates that the neutron intensity also
696   depends on the vegetation structure and the detector position relative to the vegetation.

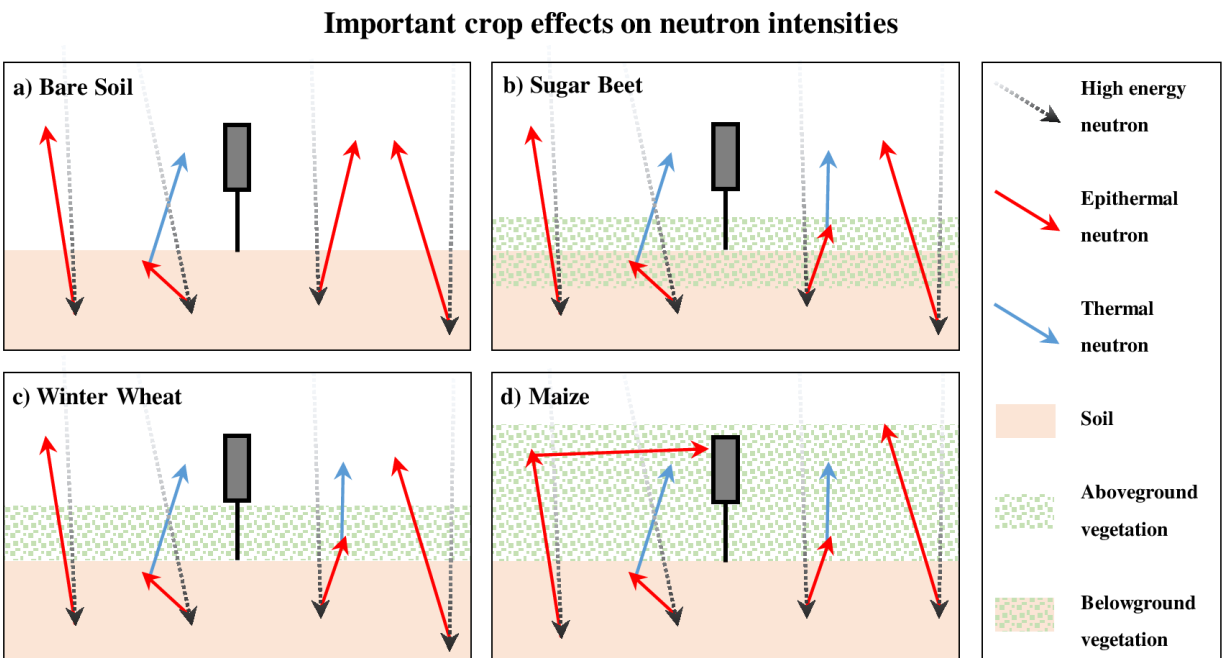**Important crop effects on neutron intensities**

Figure 14: Summary of important vegetation related processes for thermal and epithermal neutrons for (a) bare soil, (b) sugar beet, (c) winter wheat, and (d) maize.

5. Conclusions and Outlook

In our study we used sugar beet, winter wheat, and maize, to analyze the effect of crop biomass on estimating soil moisture content with CRNS. We found that correcting the influence of vegetation using local linear regression models based on the calibration parameter N_0 consistently improved the accuracy of soil moisture measurements with CRNS. The best performance in terms of RMSE was obtained when both the above- and the belowground biomass were considered for correction. When only the aboveground biomass was considered, the performance decreased when high amounts of belowground biomass were present (i.e., in the case sugar beet). The empirical linear relationship of BAATZ ET AL. (2015) also improved measurement accuracy, except for maize where the accuracy was considerably lower after correction. In contrast, a vegetation correction based on the thermal-to-epithermal neutron ratio (N_r) or thermal neutron intensity always improved the accuracy of soil moisture content measurement with CRNS. Different from results presented in earlier studies (TIAN ET AL., 2016; JAKOBI ET AL., 2018), N_r was not consistently related to changes in aboveground biomass. However, we found that the thermal neutron intensity could also be used to predict changes in the total biomass (i.e., the sum of above- and belowground biomass water equivalent - BWE_{tot}).

For future studies, we suggest to investigate the dependency of thermal neutrons on different biomass and vegetation structures in more detail. To this end, irrigation experiments or neutron transport simulations could allow for the investigation of the neutron intensities with constant soil moisture content and changing biomass/vegetation structures (and vice versa). The influence of the vegetation structure (i.e., the density of stalks, fruit bodies and the plant height) should also be investigated using neutron transport modelling. Similarly, forest sites are interesting to consider as we anticipate a different behavior of thermal neutrons in comparison to sites were all hydrogen sources are at the same height or below the detectors (ANDREASEN ET AL., 2017a; ANDREASEN ET AL., 2020; JAKOBI ET AL., 2021).

**Appendix A – Hysteresis in the sugar beet experiment**

For sugar beet, we found hysteretic behavior in the $N_r - N_0$ (Figure 7a), N_r – soil moisture content (Figure 11d) and the thermal neutron intensity – soil moisture content (Figure 12d) relationships. Here, we investigate this hysteresis in more detail. From Figure A15a-c, it can be seen that the hysteresis also occurred in the epithermal neutron - soil moisture content relationship. In this case, three stages with different slopes can be identified. The coloring indicates that the different responses were related to the growth of biomass with the largest effect from belowground biomass (e.g., Figure A15b at $E = 0.9$ and $\theta_{reference} = 0.3$). Similarly, the thermal neutron intensity was strongly influenced by belowground biomass (Figure A15e).

Figure A1 shows that the hysteresis in the epithermal neutron intensity can be effectively removed with corrections considering in-situ measured BWE_{tot}, N_r or the thermal neutron intensity, which is also indicated by the improvement in soil moisture content estimation in comparison to the bare soil calibration (i.e., calibration strategy B; see Table 3). However, the relation to soil moisture content was changed when N_r was used for correction. This may be related to the different footprints of thermal and epithermal neutrons and could possibly be accounted for by refitting the parameters p_i (Equation (9); DESILETS ET AL., 2010), as shown in earlier studies. For instance, RASCHE ET AL. (2021) found that the sum of thermal and epithermal neutrons could be used for soil moisture content estimation if p_i were refitted. In this context, it has to be noted that KÖHLI ET AL. (2021) showed that Equation (9) is over-parameterized and suggested that their reformulated equation should be much better suited for parameter fitting. However, this was beyond the scope of our study.

751
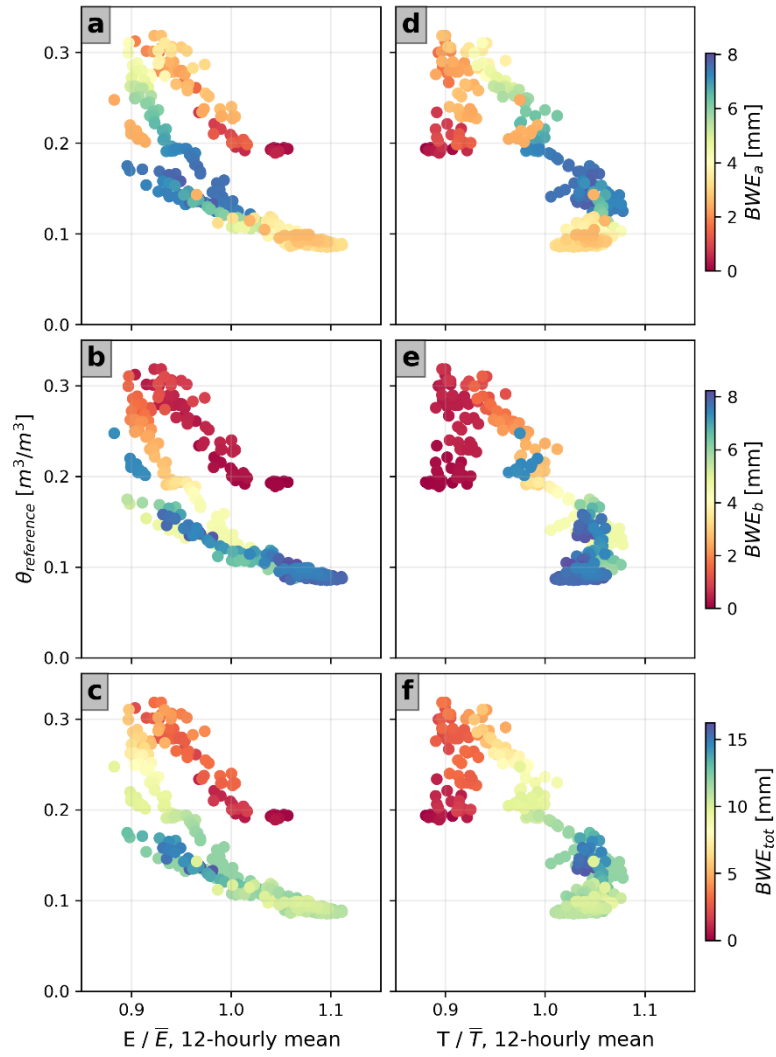
Figure A15: Relationships of the epithermal (a) – c)) and thermal neutron (d) - f)) intensities relative to their respective mean of the whole time series and reference soil moisture content for the Sugar Beet experiment. The colouring sequences indicate changes in biomass water equivalent (BWE, linearly interpolated), differentiated in aboveground BWE (BWE_a; a) and d)), belowground BWE (BWE_b; b) and e)) and the sum of above- and belowground BWE (BWE_{tot}: c) and f)).

757
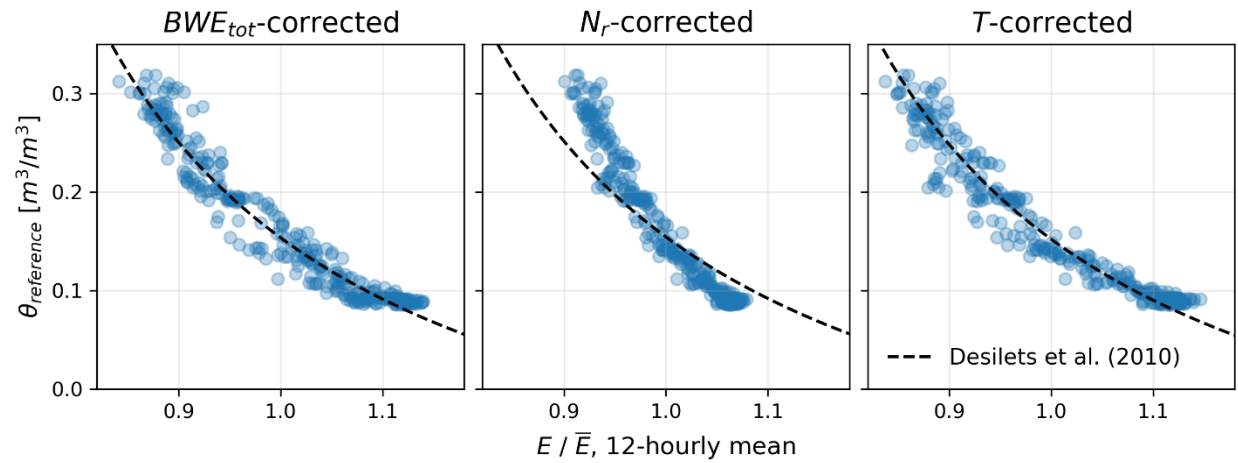
Figure A1: Relationships of the epithermal neutron intensities corrected for the influences of the sum of
above- and belowground biomass water equivalent (BWE_{tot}), the thermal-to-epithermal neutron ratio (N_r)
and the thermal neutron intensity (T) relative to their respective mean of the whole time series for sugar
beet. For comparison also Equation (9) is shown (using $f = 1$ and $N_{0,BWetot=0}$, $N_{0,Nr=0}$ and $N_{0,T=0}$, respectively).

Data availability statement

The datasets used in this study will be published on the TERENO (Terrestrial Environmental Observatories) data portal (https://ddp.tereno.net/ddp/) upon acceptance of the manuscript and until then are available from the supporting information.

Literature

ANDREASEN, M., JENSEN, K. H., ZREDA, M., DESILETS, D., BOGENA, H., AND LOOMS, M. C. (2016), Modeling cosmic ray neutron field measurements, *Water Resour. Res.*, *52*(8), 6451–6471, doi:10.1002/2015WR018236.

ANDREASEN, M., JENSEN, K. H., DESILETS, D., ZREDA, M., BOGENA, H. R., AND LOOMS, M. C. (2017a), Cosmic-ray neutron transport at a forest field site: the sensitivity to various environmental conditions with focus on biomass and canopy interception, *Hydrol. Earth Syst. Sci.*, *21*(4), 1875–1894, doi:10.5194/hess-21-1875-2017.

ANDREASEN, M., JENSEN, K. H., DESILETS, D., FRANZ, T. E., ZREDA, M., BOGENA, H. R., AND LOOMS, M. C. (2017b), Status and Perspectives on the Cosmic-Ray Neutron Method for Soil Moisture Estimation and Other Environmental Science Applications, *Vadose Zone Journal*, *16*(8), vzj2017.04.0086, doi:10.2136/vzj2017.04.0086.

ANDREASEN, M., JENSEN, K. H., BOGENA, H., DESILETS, D., ZREDA, M., AND LOOMS, M. C. (2020), Cosmic Ray Neutron Soil Moisture Estimation Using Physically Based Site-Specific Conversion Functions, *Water Resour. Res.*, *56*(11), doi:10.1029/2019WR026588.

BAATZ, R., BOGENA, H. R., HENDRICKS FRANSSEN, H.-J., HUISMAN, J. A., QU, W., MONTZKA, C., AND VEREECKEN, H. (2014), Calibration of a catchment scale cosmic-ray probe network: A comparison of three parameterization methods, *Journal of Hydrology*, *516*, 231–244, doi:10.1016/j.jhydrol.2014.02.026.

BAATZ, R., BOGENA, H. R., HENDRICKS FRANSSEN, H.-J., HUISMAN, J. A., MONTZKA, C., AND VEREECKEN, H. (2015), An empirical vegetation correction for soil water content quantification using cosmic ray probes, *Water Resour. Res.*, *51*(4), 2030–2046, doi:10.1002/2014WR016443.

BARET, F., OLIOSO, A., AND LUCIANI, J. L. (1992), Root biomass fraction as a function of growth degree days in wheat, *Plant Soil*, *140*(1), 137–144, doi:10.1007/BF00012815.

BARONI, G., AND OSWALD, S. E. (2015), A scaling approach for the assessment of biomass changes and rainfall interception using cosmic-ray neutron sensing, *Journal of Hydrology*, *525*, 264–276, doi:10.1016/j.jhydrol.2015.03.053.

BARONI, G., SCHEIFFELE, L. M., SCHRÖN, M., INGWERSEN, J., AND OSWALD, S. E. (2018), Uncertainty, sensitivity and improvements in soil moisture estimation with cosmic-ray neutron sensing, *Journal of Hydrology*, *564*, 873–887, doi:10.1016/j.jhydrol.2018.07.053.

BOGENA, H., SCHRÖN, M., JAKOBI, J., NEY, P., ZACHARIAS, S., ANDREASEN, M., BAATZ, R., BOORMAN, D., DUYGU, B. M., EGUIBAR-GALÁN, M. A., FERSCH, B., FRANKE, T., GERIS, J., GONZÁLEZ SANCHIS, M., KERR, Y., KORF, T., MENGISTU, Z., MIALON, A., NASTA, P., NITYCHORUK, J., PISINARAS, V., RASCHE, D., ROSOLEM, R., SAID, H., SCHATTAN, P., ZREDA, M., ACHLEITNER, S., ALBENTOSA-HERNÁNDEZ, E., AKYÜREK, Z., BLUME, T., DEL CAMPO, A., DIMITROVA-PETROVA, K., EVANS, J. G., FRANCES, F., GÜNTNER, A., HERRMANN, F., IWEMA, J., JENSEN, K. H., KUNSTMANN, H., LIDÓN, A., LOOMS, M. C., OSWALD, S., PANAGOPOULOS, A., PATIL, A., POWER, D., REBMANN, C., ROMANO, N., SCHEIFFELE, L. M., SENEVIRATNE, S., WELTIN, G., AND VEREECKEN, H. (in revision), COSMOS-Europe: A European Network of Cosmic-Ray Neutron Soil Moisture Sensors, doi:10.5194/essd-2021-325.

BOGENA, H. R., HERBST, M., HUISMAN, J. A., ROSENBAUM, U., WEUTHEN, A., AND VEREECKEN, H. (2010), Potential of Wireless Sensor Networks for Measuring Soil Water Content Variability, *Vadose Zone Journal*, *9*(4), 1002–1013, doi:10.2136/vzj2009.0173.

818   BOGENA, H. R., HUISMAN, J. A., BAATZ, R., HENDRICKS FRANSSEN, H.-J., AND VEREECKEN, H. (2013), Accuracy of the
819   cosmic-ray soil water content probe in humid forest ecosystems: The worst case scenario, *Water
820   Resour. Res.*, *49*(9), 5778–5791, doi:10.1002/wrcr.20463.
821   BOGENA, H. R., HUISMAN, J. A., GÜNTNER, A., HÜBNER, C., KUSCHE, J., JONARD, F., VEY, S., AND VEREECKEN, H.
822   (2015), Emerging methods for noninvasive sensing of soil moisture dynamics from field to catchment
823   scale: a review, *WIREs Water*, *2*(6), 635–647, doi:10.1002/wat2.1097.
824   BOGENA, H. R., HUISMAN, J. A., SCHILLING, B., WEUTHEN, A., AND VEREECKEN, H. (2017), Effective Calibration of
825   Low-Cost Soil Water Content Sensors, *Sensors (Basel, Switzerland)*, *17*(1), doi:10.3390/s17010208.
826   BOGENA, H. R., MONTZKA, C., HUISMAN, J. A., GRAF, A., SCHMIDT, M., STOCKINGER, M., HEBEL, C. VON, HENDRICKS-
827   FRANSSEN, H. J., VAN DER KRUK, J., TAPPE, W., LÜCKE, A., BAATZ, R., BOL, R., GROH, J., PÜTZ, T., JAKOBI, J.,
828   KUNKEL, R., SORG, J., AND VEREECKEN, H. (2018), The TERENO-Rur Hydrological Observatory: A Multiscale
829   Multi-Compartment Research Platform for the Advancement of Hydrological Science, *Vadose Zone
830   Journal*, *17*(1), 180055, doi:10.2136/vzj2018.03.0055.
831   BOGENA, H. R., HERRMANN, F., JAKOBI, J., BROGI, C., ILIAS, A., HUISMAN, J. A., PANAGOPOULOS, A., AND PISINARAS, V.
832   (2020), Monitoring of Snowpack Dynamics With Cosmic-Ray Neutron Probes: A Comparison of Four
833   Conversion Methods, *Front. Water*, *2*, doi:10.3389/frwa.2020.00019.
834   BROGI, C., HUISMAN, J. A., PÄTZOLD, S., HEBEL, C. VON, WEIHERMÜLLER, L., KAUFMANN, M. S., VAN DER KRUK, J., AND
835   VEREECKEN, H. (2019), Large-scale soil mapping using multi-configuration EMI and supervised image
836   classification, *Geoderma*, *335*, 133–148, doi:10.1016/j.geoderma.2018.08.001.
837   BROGI, C., HUISMAN, J. A., HERBST, M., WEIHERMÜLLER, L., KLOSTERHALFEN, A., MONTZKA, C., REICHENAU, T. G., AND
838   VEREECKEN, H. (2020), Simulation of spatial variability in crop leaf area index and yield using
839   agroecosystem modeling and geophysics-based quantitative soil information, *Vadose zone j.*, *19*(1),
840   doi:10.1002/vzj2.20009.
841   COOPER, H. M., BENNETT, E., BLAKE, J., BLYTH, E., BOORMAN, D., COOPER, E., EVANS, J., FRY, M., JENKINS, A.,
842   MORRISON, R., RYLETT, D., STANLEY, S., SZCZYKULSKA, M., TRILL, E., ANTONIOU, V., ASKQUITH-ELLIS, A., BALL, L.,
843   BROOKS, M., CLARKE, M. A., COWAN, N., CUMMING, A., FARRAND, P., HITT, O., LORD, W., SCARLETT, P., SWAIN,
844   O., THORNTON, J., WARWICK, A., AND WINTERBOURN, B. (2021), COSMOS-UK: national soil moisture and
845   hydrometeorology data for environmental science research, *Earth Syst. Sci. Data*, *13*(4), 1737–1757,
846   doi:10.5194/essd-13-1737-2021.
847   DESILETS, D., AND ZREDA, M. (2001), On scaling cosmogenic nuclide production rates for altitude and
848   latitude using cosmic-ray measurements, *Earth and Planetary Science Letters*, *193*(1-2), 213–225,
849   doi:10.1016/S0012-821X(01)00477-0.
850   DESILETS, D., AND ZREDA, M. (2003), Spatial and temporal distribution of secondary cosmic-ray nucleon
851   intensities and applications to in situ cosmogenic dating, *Earth and Planetary Science Letters*, *206*(1-
852   2), 21–42, doi:10.1016/S0012-821X(02)01088-9.
853   DESILETS, D., ZREDA, M., AND FERRÉ, T. P. A. (2010), Nature's neutron probe: Land surface hydrology at an
854   elusive scale with cosmic rays, *Water Resour. Res.*, *46*(11), doi:10.1029/2009WR008726.
855   DIMITROVA-PETROVA, K., GERIS, J., WILKINSON, M. E., ROSOLEM, R., VERROT, L., LILLY, A., AND SOULSBY, C. (2020),
856   Opportunities and challenges in using catchment-scale storage estimates from cosmic ray neutron
857   sensors for rainfall-runoff modelling, *Journal of Hydrology*, *586*, 124878,
858   doi:10.1016/j.jhydrol.2020.124878.
859   DONG, J., OCHSNER, T. E., ZREDA, M., COSH, M. H., AND ZOU, C. B. (2014), Calibration and Validation of the
860   COSMOS Rover for Surface Soil Moisture Measurement, *Vadose zone j.*, *13*(4), 1–8,
861   doi:10.2136/vzj2013.08.0148.

862   FERSCH, B., JAGDHUBER, T., SCHRÖN, M., VÖLKSCH, I., AND JÄGER, M. (2018), Synergies for Soil Moisture
863   Retrieval Across Scales From Airborne Polarimetric SAR, Cosmic Ray Neutron Roving, and an In Situ
864   Sensor Network, *Water Resour. Res.*, *54*(11), 9364–9383, doi:10.1029/2018WR023337.
865   FERSCH, B., FRANCKE, T., HEISTERMANN, M., SCHRÖN, M., DÖPPER, V., JAKOBI, J., BARONI, G., BLUME, T., BOGENA,
866   H., BUDACH, C., GRÄNZIG, T., FÖRSTER, M., GÜNTNER, A., HENDRICKS FRANSSEN, H.-J., KASNER, M., KÖHLI, M.,
867   KLEINSCHMIT, B., KUNSTMANN, H., PATIL, A., RASCHE, D., SCHEIFFELE, L., SCHMIDT, U., SZULC-SEYFRIED, S.,
868   WEIMAR, J., ZACHARIAS, S., ZREDA, M., HEBER, B., KIESE, R., MARES, V., MOLLENHAUER, H., VÖLKSCH, I., AND
869   OSWALD, S. (2020), A dense network of cosmic-ray neutron sensors for soil moisture observation in a
870   highly instrumented pre-Alpine headwater catchment in Germany, *Earth Syst. Sci. Data*, *12*(3), 2289–
871   2309, doi:10.5194/essd-12-2289-2020.
872   FRANZ, T. E., ZREDA, M., FERRE, T. P. A., ROSOLEM, R., ZWECK, C., STILLMAN, S., ZENG, X., AND SHUTTLEWORTH, W. J.
873   (2012), Measurement depth of the cosmic ray soil moisture probe affected by hydrogen from various
874   sources, *Water Resour. Res.*, *48*(8), doi:10.1029/2012WR011871.
875   FRANZ, T. E., ZREDA, M., FERRE, T. P. A., AND ROSOLEM, R. (2013a), An assessment of the effect of horizontal
876   soil moisture heterogeneity on the area-average measurement of cosmic-ray neutrons, *Water
877   Resour. Res.*, *49*(10), 6450–6458, doi:10.1002/wrcr.20530.
878   FRANZ, T. E., ZREDA, M., ROSOLEM, R., HORNBUCKLE, B. K., IRVIN, S. L., ADAMS, H., KOLB, T. E., ZWECK, C., AND
879   SHUTTLEWORTH, W. J. (2013b), Ecosystem-scale measurements of biomass water using cosmic ray
880   neutrons, *Geophys. Res. Lett.*, *40*(15), 3929–3933, doi:10.1002/grl.50791.
881   FUCHS, H. (2016), Effects of biomass on soil moisture measurements using cosmic-ray neutron probes:
882   Master Thesis. Radboud University, the Netherlands and University of Duisburg-Essen, Germany.
883   HAWDON, A., MCJANNET, D., AND WALLACE, J. (2014), Calibration and correction procedures for cosmic-ray
884   neutron soil moisture probes located across Australia, *Water Resour. Res.*, *50*(6), 5029–5043,
885   doi:10.1002/2013WR015138.
886   JAKOBI, J., HUISMAN, J. A., VEREECKEN, H., DIEKKRÜGER, B., AND BOGENA, H. R. (2018), Cosmic Ray Neutron
887   Sensing for Simultaneous Soil Water Content and Biomass Quantification in Drought Conditions,
888   *Water Resour. Res.*, *54*(10), 7383–7402, doi:10.1029/2018WR022692.
889   JAKOBI, J., HUISMAN, J. A., SCHRÖN, M., FIEDLER, J., BROGI, C., VEREECKEN, H., AND BOGENA, H. R. (2020), Error
890   Estimation for Soil Moisture Measurements With Cosmic Ray Neutron Sensing and Implications for
891   Rover Surveys, *Front. Water*, *2*, doi:10.3389/frwa.2020.00010.
892   JAKOBI, J., HUISMAN, J. A., KÖHLI, M., RASCHE, D., VEREECKEN, H., AND BOGENA, H. R. (2021), The Footprint
893   Characteristics of Cosmic Ray Thermal Neutrons, *Geophys Res Lett*, *48*(15),
894   doi:10.1029/2021GL094281.
895   KNOLL, G. F. (2010), *Radiation detection and measurement*, 4th ed., xxvi, 830, John Wiley, Hoboken N.J.
896   KÖHLI, M., SCHRÖN, M., ZREDA, M., SCHMIDT, U., DIETRICH, P., AND ZACHARIAS, S. (2015), Footprint
897   characteristics revised for field-scale soil moisture monitoring with cosmic-ray neutrons, *Water
898   Resour. Res.*, *51*(7), 5772–5790, doi:10.1002/2015WR017169.
899   KÖHLI, M., WEIMAR, J., SCHRÖN, M., BAATZ, R., AND SCHMIDT, U. (2021), Soil Moisture and Air Humidity
900   Dependence of the Above-Ground Cosmic-Ray Neutron Intensity, *Front. Water*, *2*,
901   doi:10.3389/frwa.2020.544847.
902   KORRES, W., REICHENAU, T. G., FIENER, P., KOYAMA, C. N., BOGENA, H. R., CORNELISSEN, T., BAATZ, R., HERBST, M.,
903   DIEKKRÜGER, B., VEREECKEN, H., AND SCHNEIDER, K. (2015), Spatio-temporal soil moisture patterns – A
904   meta-analysis using plot to catchment scale data, *Journal of Hydrology*, *520*, 326–341,
905   doi:10.1016/j.jhydrol.2014.11.042.

906 Li, D., Schrön, M., Köhli, M., Bogena, H., Weimar, J., Jiménez Bello, M. A., Han, X., Martínez Gimeno, M. A.,
907   Zacharias, S., Vereecken, H., and Hendricks Franssen, H.-J. (2019), Can Drip Irrigation be Scheduled
908   with Cosmic-Ray Neutron Sensing?, *Vadose zone j.*, *18*(1), 190053, doi:10.2136/vzj2019.05.0053.
909 Mokany, K., Raison, R. J., and Prokushkin, A. S. (2006), Critical analysis of root : shoot ratios in terrestrial
910   biomes, *Global Change Biology*, *12*(1), 84–96, doi:10.1111/j.1365-2486.2005.001043.x.
911 Rasche, D., Köhli, M., Schrön, M., Blume, T., and Güntner, A. (2021), Towards disentangling
912   heterogeneous soil moisture patterns in cosmic-ray neutron sensor footprints, *Hydrol. Earth Syst.*
913   *Sci.*, *25*(12), 6547–6566, doi:10.5194/hess-25-6547-2021.
914 Rivera Villarreyes, C. A., Baroni, G., and Oswald, S. E. (2011), Integral quantification of seasonal soil
915   moisture changes in farmland by cosmic-ray neutrons, *Hydrol. Earth Syst. Sci.*, *15*(12), 3843–3859,
916   doi:10.5194/hess-15-3843-2011.
917 Rosolem, R., Shuttleworth, W. J., Zreda, M., Franz, T. E., Zeng, X., and Kurc, S. A. (2013), The Effect of
918   Atmospheric Water Vapor on Neutron Count in the Cosmic-Ray Soil Moisture Observing System,
919   *Journal of Hydrometeorology*, *14*(5), 1659–1671, doi:10.1175/JHM-D-12-0120.1.
920 Rudolph, S., van der Kruk, J., Hebel, C. von, Ali, M., Herbst, M., Montzka, C., Pätzold, S., Robinson, D. A.,
921   Vereecken, H., and Weihermüller, L. (2015), Linking satellite derived LAI patterns with subsoil
922   heterogeneity using large-scale ground-based electromagnetic induction measurements, *Geoderma*,
923   *241-242*, 262–271, doi:10.1016/j.geoderma.2014.11.015.
924 Scheiffele, L. M., Baroni, G., Franz, T. E., Jakobi, J., and Oswald, S. E. (2020), A profile shape correction to
925   reduce the vertical sensitivity of cosmic-ray neutron sensing of soil moisture, *Vadose zone j.*, *19*(1),
926   doi:10.1002/vzj2.20083.
927 Schrön, M., Köhli, M., Scheiffele, L., Iwema, J., Bogena, H. R., Lv, L., Martini, E., Baroni, G., Rosolem, R.,
928   Weimar, J., Mai, J., Cuntz, M., Rebmann, C., Oswald, S. E., Dietrich, P., Schmidt, U., and Zacharias, S.
929   (2017), Improving calibration and validation of cosmic-ray neutron sensors in the light of spatial
930   sensitivity, *Hydrol. Earth Syst. Sci.*, *21*(10), 5009–5030, doi:10.5194/hess-21-5009-2017.
931 Sigouin, M. J., Dyck, M., Si, B. C., and Hu, W. (2016), Monitoring soil water content at a heterogeneous oil
932   sand reclamation site using a cosmic-ray soil moisture probe, *Journal of Hydrology*, *543*, 510–522,
933   doi:10.1016/j.jhydrol.2016.10.026.
934 Tian, Z., Li, Z., Liu, G., Li, B., and Ren, T. (2016), Soil water content determination with cosmic-ray neutron
935   sensor: Correcting aboveground hydrogen effects with thermal/fast neutron ratio, *Journal of*
936   *Hydrology*, *540*, 923–933, doi:10.1016/j.jhydrol.2016.07.004.
937 Topp, G. C., Davis, J. L., and Annan, A. P. (1980), Electromagnetic determination of soil water content:
938   Measurements in coaxial transmission lines, *Water Resour. Res.*, *16*(3), 574–582,
939   doi:10.1029/WR016i003p00574.
940 Vather, T., Everson, C. S., and Franz, T. E. (2020), The Applicability of the Cosmic Ray Neutron Sensor to
941   Simultaneously Monitor Soil Water Content and Biomass in an Acacia mearnsii Forest, *Hydrology*,
942   *7*(3), 48, doi:10.3390/hydrology7030048.
943 Weihermüller, L., Huisman, J. A., Lambot, S., Herbst, M., and Vereecken, H. (2007), Mapping the spatial
944   variation of soil water content at the field scale with different ground penetrating radar techniques,
945   *Journal of Hydrology*, *340*(3-4), 205–216, doi:10.1016/j.jhydrol.2007.04.013.
946 Zreda, M., Desilets, D., Ferré, T. P. A., and Scott, R. L. (2008), Measuring soil moisture content non-
947   invasively at intermediate spatial scale using cosmic-ray neutrons, *Geophys. Res. Lett.*, *35*(21),
948   doi:10.1029/2008GL035655.

949   Zreda, M., Shuttleworth, W. J., Zeng, X., Zweck, C., Desilets, D., Franz, T., and Rosolem, R. (2012),
950   COSMOS: the COsmic-ray Soil Moisture Observing System, *Hydrol. Earth Syst. Sci.*, *16*(11), 4079–
951   4099, doi:10.5194/hess-16-4079-2012.
952   Zweck, C., Zreda, M., and Desilets, D. (2013), Snow shielding factors for cosmogenic nuclide dating
953   inferred from Monte Carlo neutron transport simulations, *Earth and Planetary Science Letters*, *379*,
954   64–71, doi:10.1016/j.epsl.2013.07.023.
955